Loss of uniqueness of numerical solutions of the borehole problem modelled with enhanced media

Yannick Sieffert, Samah Al Holo, René Chambon

International Journal of Solids and Structures 46 (2009) 3173–3197

Contents lists available at ScienceDirect

International Journal of Solids and Structures

journal homepage: www.elsevier.com/locate/ijsolstr

Loss of uniqueness of numerical solutions of the borehole problem modelled with enhanced media

Y. Sieffert, S. Al Holo, R. Chambon *

Grenoble Université Joseph-Fourier, Laboratoire 3S-R, INP, CNRS, B.P. 53X, 38041 Grenoble Cedex, France

ARTICLE INFO

Article history:
Received 4 April 2008
Received in revised form 20 March 2009
Available online 3 May 2009

Keywords:
Localization
Second gradient model
Excavation
Non uniqueness
Borehole

ABSTRACT

It is well known that, initial boundary value problems involving constitutive equations modeling the degradation of the strength of materials are not well posed, which renders computations questionable. To overcome this issue it is necessary to enhance the models by incorporating some internal length. It has been shown that such an enhancement restores the objectivity of the computation as spurious mesh dependency is avoided. However, at least for simple problems (e.g. one dimensional ones), it has been proven that uniqueness of the underlying mathematical problem itself is not restored. Moreover numerical modeling of element tests yields several solutions. This paper demonstrates that several numerical solutions can be obtained also for less simple problems, namely the borehole problems. Even when a defect is introduced in the computed problems, different numerical solutions are found. Contrary to the one dimensional problem there is no proof that this loss of uniqueness comes from the underlying mathematical problem. It is our opinion that this is an inherent property of initial boundary value problems where, broadly speaking, strong degradation of the mechanical properties is modeled. In any case, it is necessary to be aware of this issue. For problems involving constitutive equation modeling strength degradation, it is important to try to find other solutions than the one obtained by using routinely a numerical code. The failure patterns of the different solutions found are however similar to experimental observations. This possible loss of uniqueness can then be seen as a counterpart of the difficulties encountered when attempting to reproduce experiments. This is crucial when dealing with geomaterials.

1. Introduction

Despite many advances in recent years, modeling problems that involve a degradation of the mechanical properties of materials remains a challenging task, especially for geomaterials. Experimental results show that under shearing the strength of most materials decreases. This degradation can be due to increasing porosity in granular materials, or by development of micro fractures in cohesive materials (rocks and concrete). In order to model such a behavior, constitutive equations involving softening are used. This induces many problems for initial boundary value problems that involve such constitutive equations. As a consequence, the corresponding rate boundary value problems and thus also the initial boundary value problems, are no longer well posed. Computations with such models are questionable as demonstrated by the observed mesh dependency of the computed solutions.

It is now well known that in order to remedy to the difficulties highlighted above, the use of enhanced models incorporating some internal length is necessary. Many models have been proposed since the pioneering works of Aifantis (1984) and Pijaudier-Cabot and Bažant (1987). It is not our intention in this introduction to review these enhanced models, but it is necessary to clearly present the kind of model used in this paper. Broadly speaking, there are non local models that involve an averaging over a prescribed area (Pijaudier-Cabot and Bažant, 1987) and models involving gradients. For the latter it is useful to distinguish between the models using the gradient of some internal variables (Aifantis, 1984) and the ones based on general enhanced models, where kinematics is enriched independently of the kind of constitutive equation used. The latter models are based on the pioneering work of Mindlin (1964, 1965), Germain (1973a,b). These models are called local second gradient models in this paper because the constitutive equation remains local, even if it incorporates the second gradient of the displacements. The computations reported in the paper use such local second gradient models. All the enhanced models produce objective computations provided the mesh size is less than some internal length of the model.

However it has not yet been proven that the solutions of initial boundary value problems built up with the aforementioned enhanced models are unique. Similarly there is no proof that for a given state, the solution of the corresponding rate boundary value problem is unique if some softening behavior is incorporated into

* Corresponding author.
E-mail addresses: yannick.sieffert@ujf-grenoble.fr (Y. Sieffert), samah.alholo@hmg.inpg.fr (S. Al Holo), rene.chambon@ujf-grenoble.fr (R. Chambon).

0020-7683/$ - see front matter © 2009 Elsevier Ltd. All rights reserved.
doi:10.1016/j.ijsolstr.2009.04.014

the constitutive equation. The only proof about such a problem has been established by Chambon and Moullet (2004), but the sufficient conditions of this proof implies no softening. On the contrary several solutions have been exhibited by Chambon et al. (1996, 1998) for a one dimensional problem. In these papers, analytical solutions are developed. Uniqueness or non uniqueness depends on the ratio of the size of the studied domain with respect to the internal length of the model. If this ratio is small, then solution can be unique, but if this ratio is sufficiently large, then several solutions can be found. Unfortunately we have not yet succeeded to extend this result to less simple problems. For the one dimensional problem, studied by Chambon et al. (1998), besides the analytical solutions, a numerical study was carried out. This numerical analysis was based on classical time discretization, and for every time step Newton's method was used to solve the corresponding non linear equations. It was demonstrated that it is possible to retrieve all the analytical solutions, only by using different starting guesses in the Newton's method, generalizing the method already proposed for usual continuum mechanics problems (see Chambon et al., 2001b).

Such numerical experiments were done for the computation of biaxial tests. Such tests are very important since they are currently used to identify the parameters of the classical (here classical means related to first gradient theories) constitutive equations, but with an assumption of homogeneity. Several numerical solutions with different orientated bands of localized deformation have been presented in Chambon and Moullet (2004). Furthermore solutions for which the localized deformation bands are active at some time and inactive for subsequent periods during the test have been shown in Bésuelle et al. (2006). These different numerical solutions have been qualitatively compared with experiment results and they can be related with loss of reproducibility of experiments (Bésuelle et al., 2006).

The objective of the present paper is to go a step further and to carry out similar numerical experiments for a less simple problem, namely the borehole problem. This problem has important applications in petroleum engineering and in nuclear waste disposal. Due to its importance the borehole failure problem has been tackled with different methods over the years. The present work uses a local second gradient method in which the classical part involves softening. It is not our intention to model a specific experiment, but to search if it is possible to find several objective numerical solutions for the same (less simple than the already studied ones) initial boundary value problem. The methods used to search alternative solutions are the ones first proposed in Chambon et al. (2001b), for classical problems, and generalized for second gradient models in Chambon and Moullet (2004), as mentioned above. It has to be emphasized that these results do not prove anything concerning the underlying mathematical problem. Moreover, even if we believe that these different numerical solutions are related with different solutions of the mathematical problem, it is likely that not all the bifurcated solutions are found. However this method gives us crucial results concerning the limitation of numerical computations of softening materials even when enhanced models are used.

The sequence of presentation is as follows. A first part provides a short presentation of the local second gradient model used. Starting from is the virtual work principle as developed by Germain (1973a), the model used in the following computations is detailed. It has been chosen to be the simplest possible model. The parameters used are then outlined before presenting briefly, the numerical implementation of the model.

In the second part of the paper, the specific aspects of the borehole problem are given. First the general assumptions and the geometrical aspects are described. The history of boundary conditions that defines completely the initial boundary value problem is then given. Finally the different meshes used in the numerical experiments are presented.

Preliminary results of the numerical simulation are given in the third section. The goal of this modeling is to check the objectivity of the numerical solutions. This task is not straightforward as comparison of results obtained with different meshes can be a little bit challenging due to the non uniqueness of solutions.

The fourth section is the heart of this work. Here the numerical experiments performed are presented with some details. It is demonstrated that several numerical solutions can be found. As already seen in Chambon et al. (1996, 1998), small differences in any *numerical* input data can yield different solutions. This section finishes with a study of the influence of defects in the *physical* data on the results of the computations. In some cases this does not restore the uniqueness of solutions.

In the final section some concluding remarks based on a qualitative comparison with some experimental data found in the literature are given.

Before starting, it is important to specify the main limitations of this work. The first restriction of this study is that we deal only with quasi-static problems. This means that we neglect the inertia terms and the so-called micro-inertia effects as well. Furthermore for the sake of simplicity, hydro mechanical coupling is discarded and the geomaterial is assumed to be monophasic. Finally, we do not consider couple body forces, only classical ones. However large strain computations are run and the results are plotted in the current configuration without any magnification of the displacements.

2. Local second gradient models

Let us first recall the main features of local second gradient models. An enriched kinematical description of the continuum is used. In addition to the displacement field, u_i, a second order tensor, the so-called micro kinematic gradient ν_{ij}, is introduced. This yields media with micro structure as defined by Mindlin (1964) or Germain (1973b). Starting from these models, and introducing the constraint equating the micro kinematic gradient ν_{ij} and the gradient of the displacement field, u_i (see Eq. (1)), yields the local second gradient models as studied for instance in Chambon et al. (2001a),

$$\nu_{ij} = \frac{\partial u_i}{\partial x_j}. \tag{1}$$

2.1. Virtual work equation and balance equations of local second gradient models

The virtual work equation written in the current configuration reads:

$$\int_\Omega \left(\sigma_{ij}\epsilon^*_{ij} + \Sigma_{ijk}\frac{\partial^2 u^*_i}{\partial x_j \partial x_k} \right) dv = \int_\Omega G_i u^*_i \, dv + \int_{\partial\Omega} (p_i u^*_i + P_i D u^*_i) ds, \tag{2}$$

where σ_{ij} is the Cauchy stress, u^*_i is a kinematically admissible virtual displacement field, ϵ^*_{ij} is the virtual macro strain rate (i.e. $\epsilon^*_{ij} = \frac{1}{2}\left(\frac{\partial u^*_i}{\partial x_j} + \frac{\partial u^*_j}{\partial x_i}\right)$), x_i are the current coordinates, Σ_{ijk} is the so called double stress, the dual static variable associated to the second gradient of the virtual displacement. G_i is the body force by unit volume (as mentioned in the introduction, couple body forces are not considered), p_i and P_i are two independent variables which can be prescribed on the boundary and Dq denotes the normal derivative of any quantity q (for instance $Du_i = n_k \partial u_i / \partial x_k$ where n_k is the normal to the assumed $C1$ boundary).

It is straightforward to show that Eq. (2) yields the balance equation

$$\frac{\partial \sigma_{ij}}{\partial x_j} - \frac{\partial^2 \Sigma_{ijk}}{\partial x_j \partial x_k} + G_i = 0, \tag{3}$$

and the boundary conditions:

$$\sigma_{ij} n_j - n_k n_j D\Sigma_{ijk} - \frac{D\Sigma_{ijk}}{Dx_k} n_j - \frac{D\Sigma_{ijk}}{Dx_j} n_k + \frac{Dn_l}{Dx_l} \Sigma_{ijk} n_j n_k - \frac{Dn_j}{Dx_k} \Sigma_{ijk} = p_i, \tag{4}$$

$$\Sigma_{ijk} n_j n_k = P_i, \tag{5}$$

where Dq/Dx_j denotes the tangential derivatives of any quantity q:

$$\frac{Dq}{Dx_j} = \frac{\partial q}{\partial x_j} - n_j Dq. \tag{6}$$

2.2. Constitutive equation

2.2.1. General framework

Let us generalize the classical way of building constitutive equations of Truesdell and Noll (1943). The generalized stresses $\sigma_{ij}, \Sigma_{ijk}$ denoted generically S are known in every point of the material if the history of the whole kinematics (including the second gradient history) denoted generically E is known at the same point. The history of the whole kinematics gives the generalized stresses.

$$S(t^f) = \Upsilon(E(t), t \in [0, t^f]), \tag{7}$$

where here t is the time and t^f a given time. This equation defines a local continuum because the generalized stress depends only on the local kinematic history. This prompts us to call such a model a local second gradient model.

Such a constitutive equation can also be defined in a rate form. For objectivity requirements, the Jaumann rate of the Cauchy stress,

$$\overset{\nabla}{\sigma}_{ik} = \dot{\sigma}_{ik} - \sigma_{jk}\dot{\omega}_{ji} - \sigma_{ij}\dot{\omega}_{jk}, \tag{8}$$

and of the double stress,

$$\overset{\nabla}{\Sigma}_{ijk} = \dot{\Sigma}_{ijk} + \Sigma_{ljk}\dot{\omega}_{li} + \Sigma_{imk}\dot{\omega}_{mj} + \Sigma_{ijp}\dot{\omega}_{pk}, \tag{9}$$

where $\dot{\omega}_{ij} = \frac{1}{2}\left(\frac{\partial \dot{u}_i}{\partial x_j} - \frac{\partial \dot{u}_j}{\partial x_i}\right)$ is the spin tensor, can be used and defined as some functions of the state parameters and some suitable rate of the whole local kinematics.

2.2.2. The model used

The constitutive model used in this paper is the one used by Matsushima et al. (2002), Chambon and Moullet (2004), and

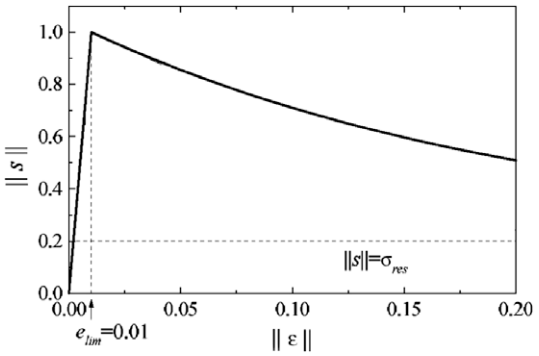

Fig. 1. Classical part of the constitutive relation.

Table 1
Description of the three meshes used.

Name	Element around perimeter	Nodes	Elements	Degrees of freedom
Coarse	32	1733	448	5952
Fine	64	6528	1664	22354
Very fine	128	23808	6016	82944

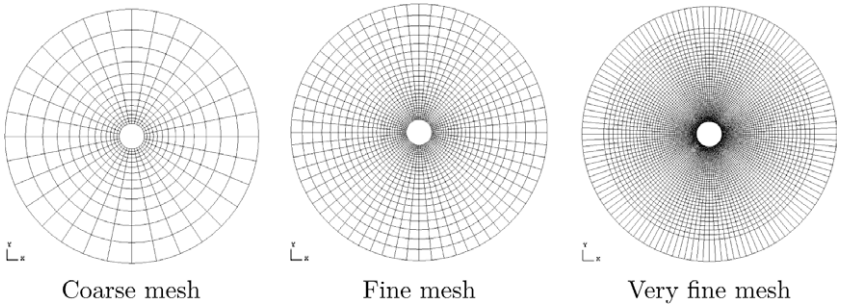

Fig. 2. The three meshes used.

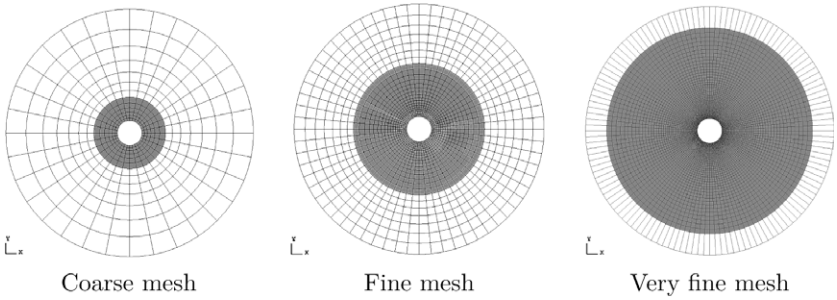

Fig. 3. Areas where localization is well modelled for the three meshes.

Bésuelle et al. (2006). It is a hypoelastoplastic model for which, the classical part of the constitutitve equation giving the stress and the other part giving the double stress, are decoupled.

In the following applications, the classical part is a Von Mises model involving softening. The isotropic (hypoelastic) part is defined as:

$$\dot{\sigma} = 3K\dot{e}, \tag{10}$$

where $\dot{\sigma}$ is the mean stress rate, $\dot{e}$ the mean strain rate and K the bulk modulus. The (elasto plastic) deviatoric part is defined as:

$$\overset{\nabla}{s}_{ij} = \begin{cases} 2G_1\,\dot{\varepsilon}_{ij} & (\|\varepsilon\| \leqslant e_{lim}) \\ 2G_1\left(\dot{\varepsilon}_{ij} - \frac{G_1-G_2}{G_1}\frac{s_{kl}\dot{\varepsilon}_{kl}}{\|s\|^2}s_{ij}\right) & (\|\varepsilon\| > e_{lim}) \end{cases}, \tag{11}$$

where, $\overset{\nabla}{s}_{ij}$ is the Jaumann rate of the deviatoric Cauchy stress tensor, $\dot{\varepsilon}_{ij}$ is the deviatoric strain rate, G_1 and G_2 are the shear moduli before peak and after peak, respectively, $\|\varepsilon\|$ is the second invariant of the Green–Lagrange deformation tensor, e_{lim} is a parameter of the model corresponding to the second invariant of the strain related with the initial (before softening) value of the peak deviatoric stress.

The bulk modulus K is assumed to be constant. The elastic shear modulus for elastic loading and unloading is assumed to be constant. However an exponential function is assumed to govern the shear modulus after the yield point so that the stress could reach smoothly a residual value,

$$G_2 = \overline{G}_2 \exp\left(\frac{\overline{G}_2}{2G_1 e_{lim} - \sigma_{res}}(\|\varepsilon\| - e_{lim})\right), \tag{12}$$

where $\overline{G}_2$ is the value of the shear modulus just after yielding and σ_{res} is the residual deviatoric stress. Fig. 1 shows the evolution of the stress deviator as a function of the strain deviator for a monotonic loading.

The second gradient part (decoupled from the classical one) is a very particular case of the more general isotropic linear relation derived by Mindlin (1964), involving six parameters corresponding to five independent coefficients. For simplification, we use only one parameter namely D following Bésuelle et al. (2006).

$$\begin{bmatrix} \overset{\nabla}{\Sigma}_{111} \\ \overset{\nabla}{\Sigma}_{112} \\ \overset{\nabla}{\Sigma}_{121} \\ \overset{\nabla}{\Sigma}_{122} \\ \overset{\nabla}{\Sigma}_{211} \\ \overset{\nabla}{\Sigma}_{212} \\ \overset{\nabla}{\Sigma}_{221} \\ \overset{\nabla}{\Sigma}_{222} \end{bmatrix} = \begin{bmatrix} D & 0 & 0 & 0 & 0 & D/2 & D/2 & 0 \\ 0 & D/2 & D/2 & 0 & -D/2 & 0 & 0 & D/2 \\ 0 & D/2 & D/2 & 0 & -D/2 & 0 & 0 & D/2 \\ 0 & 0 & 0 & D & 0 & -D/2 & -D/2 & 0 \\ 0 & -D/2 & -D/2 & 0 & D & 0 & 0 & 0 \\ D/2 & 0 & 0 & -D/2 & 0 & D/2 & D/2 & 0 \\ D/2 & 0 & 0 & -D/2 & 0 & D/2 & D/2 & 0 \\ 0 & D/2 & D/2 & 0 & 0 & 0 & 0 & D \end{bmatrix} \times \begin{bmatrix} \frac{\partial \dot{v}_{11}}{\partial x_1} \\ \frac{\partial \dot{v}_{11}}{\partial x_2} \\ \frac{\partial \dot{v}_{12}}{\partial x_1} \\ \frac{\partial \dot{v}_{12}}{\partial x_2} \\ \frac{\partial \dot{v}_{21}}{\partial x_1} \\ \frac{\partial \dot{v}_{21}}{\partial x_2} \\ \frac{\partial \dot{v}_{22}}{\partial x_1} \\ \frac{\partial \dot{v}_{22}}{\partial x_2} \end{bmatrix}, \tag{13}$$

where $\dot{v}_{ij}$ is the material time derivative of v_{ij}, and $\overset{\nabla}{\Sigma}_{ijk}$ is the Jaumann time derivative of the double stress as defined above.

2.2.3. Parameters of the model

It is not our intention to compute a particular soft rock. The constitutive parameters, given hereafter, are chosen because they render the computations tractable. Especially the internal length embedded in the values of $G_1, \overline{G}_2$ and D is larger enough with respect to the mesh size (see Section 3.3).

Table 2
Input data for the numerical computations discussed.

Name	Mesh	Max step size	Confining pressure at random initialization	Type of solution	Imperfection	Number of bands
AxiC	32	0.1	–	Axisymmetrical	–	–
AxiF	64	0.1	–	Axisymmetrical	–	–
AxiVF	128	0.07	–	Axisymmetrical	–	–
BandC7	32	0.04	–	Periodic bands	–	7
BandC8	32	0.16	–	Periodic bands	–	8
BandC8bis	32	0.01	–	Periodic bands	–	8
BandF10	64	0.01	18%	Periodic bands	–	10
BandF10bis	64	0.01	18%	Periodic bands	–	10
BandF11	64	0.04	–	Periodic bands	–	11
BandVF11	128	0.04	–	Periodic bands	–	11
BandVF12	128	0.02	–	Periodic bands and crossing bands	–	12
CrosF	64	0.02	–	Crossing bands	–	12
CrosVF	128	0.01	–	Crossing bands	–	13
WeakC1	32	0.004	–	Periodic bands	Yes	8
WeakC2	32	0.16	–	Periodic bands	Yes	10
WeakF1	64	0.004	–	Periodic bands	Yes	–
WeakF2	64	0.04	–	Periodic bands	Yes	11
WeakVF1	128	0.004	–	Periodic bands	Yes	11
WeakVF2	128	0.04	–	Periodic bands	Yes	10

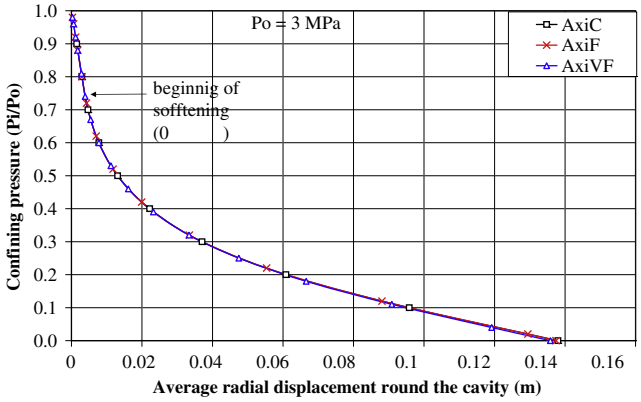

Fig. 4. Internal pressure as a function of the internal radial displacement.

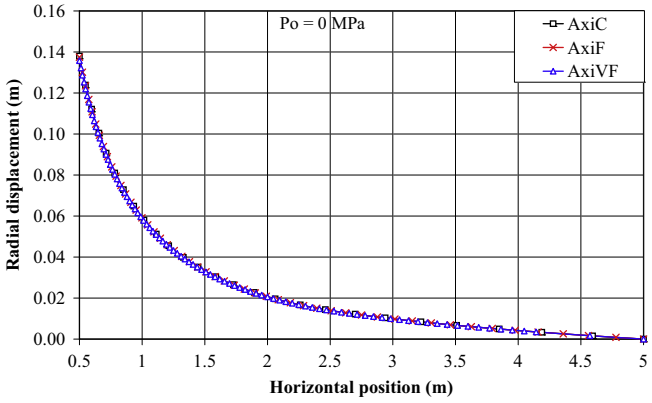

Fig. 5. Radial displacement of a radius at the end of loading as a function of the distance to the center.

If this model has to be used for a given materials, only G_1 and K which are elastic parameter are to some extend easy to calibrate. But the determination of $\overline{G}_2$ and D, linked to softening and consequently to localization, can be achieved only with field measurement experiments such as those presented by Desrues et al. (1996) or Lenoir et al. (2007) for instance. In the following computations the constitutive parameters chosen are:

$$G_1 = 50\,\text{MPa}, \quad \overline{G}_2 = -2\,\text{MPa}, \quad e_{lim} = 0.01,$$
$$K = -97\,\text{MPa}, \quad \sigma_{res} = 0.2\,\text{MPa}, \quad D = 500\,\text{N}. \tag{14}$$

They are the same as the ones used by Chambon and Moullet (2004), Al Holo (2005).

2.3. Numerical methods

All the following computations are performed using the large strain finite element code Lagamine initially developed at Liège in Belgium by Charlier (1987). The elements and the constitutive equation used have been implemented by Bésuelle et al. (2006). Giving a loading history, the computations are done step by step using an updated Lagrangian scheme and equations corresponding to each step are solved with a full Newton method using a numerical consistent tangent stiffness matrix. In order to work with C0 elements, displacements and gradient of displacement are used as independent variables. Their relation is enforced in a weak form using Lagrange multipliers. We want however to emphasize here that the elements are basically Q8 elements integrated with four Gauss points in order to avoid plastic locking. All the other details about the numerical treatment and the elements used can be found in Matsushima et al. (2002) or in Bésuelle et al. (2006) and are not recalled in this paper.

In order to find several numerical solutions for the same initial boundary value problem, the method proposed by Chambon et al. (2001b) for classical media and generalized for enhanced media by Chambon and Moullet (2004), Bésuelle et al. (2006) has been used in most of the cases. For other cases different *numerical* input data (see Section 3.4) are sufficient to find properly converged different solutions.

3. The numerical problem solved

3.1. The borehole problem

In waste disposal or petroleum engineering, it is important to properly model the drilling of a borehole in a natural soft rocks. These materials undergo drastic strength degradation that can induce damage in the walls of a borehole. In order to model such a problem the borehole is assumed to be sufficiently long allowing the assumption of a plane strain problem. The computed domain is then the area in between two circles sharing the same center. A ratio of 10 between the external radius and the inner radius of the studied domain has been chosen.

3.2. History of boundary conditions

The initial stress state is homogeneous and isotropic. The initial hydrostatic stress denoted σ_0 is applied. In all the computations $\sigma_0 = 3\,\text{MPa}$. The history of boundary conditions is the following. The displacements of the external boundary are prescribed equal to zero. The drilling itself is modelled here by a decrease of the internal pressure from the initial value 3 MPa to 0. This means that the corresponding boundary conditions p_i as defined in Eq. (4) is:

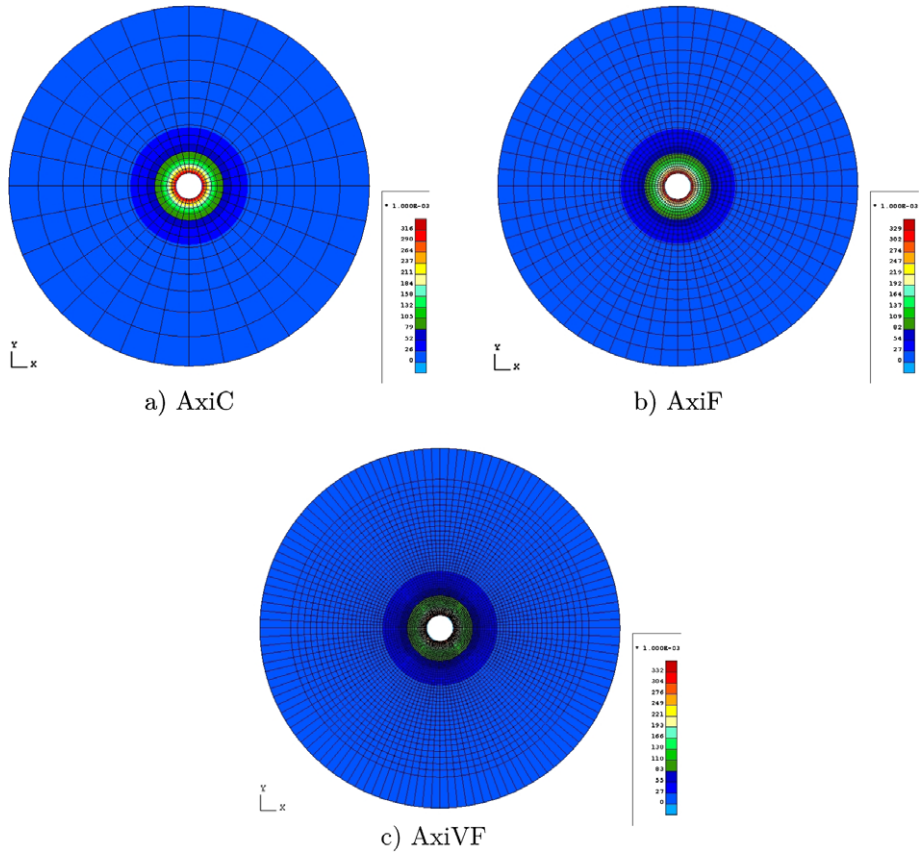

Fig. 6. Second Invariant of deformation for the axisymmetrical solutions (end of the computation).

$p_i = pn_i$ where n_i is the normal to the boundary. The loading parameter used in studying the forthcoming computations (usually called time even if all these computations are rate independent) is the ratio between the current value of the inner pressure and its initial value, it varies consequently from 1 to 0. The current *time* is then given as a decreasing number and the magnitude of the time steps is given as an adimensional number.

For the additional boundary conditions, the ones defined in Eq. (5), we use the so called natural boundary conditions which means that for the inner boundary as well as for the outer one $P_i = 0$.

3.3. Geometry and meshes

As already mentioned, we chose a ratio between the external radius and the internal one equal to 10. The internal radius is equal to 0.5 m. We checked that the variations of the external stress during the computation are negligible for all the computations performed.

A possible solution of the problem is axisymmetric. Since our goal is to study the loss of uniqueness of the solutions, we made no assumption about the solution and the complete problem is computed. However in order not to induce bias into the computations, we use meshes as symmetric as possible. This means that our meshes are build by repeating identical angular sectors.

In order to use elements close to square, the size of the elements increases with respect to the distance to the center of the circles defining the boundaries. This has been done except for the external part of the more refined mesh in order to avoid a problem with a too large number of degrees of freedom. The elements are then larger for areas far from the center. Since the localized area starts close to the inner radius, this size is not a problem for the incipient localization, but we have to keep in mind this restriction for a completely developed pattern of localized bands.

Three different meshes are used. The first mesh is a coarse mesh with 32 elements around the cavity. The second mesh is a fine mesh with 64 elements and the last mesh is a very fine with 128 elements. Details of these meshes are presented in Table 1 and the meshes themselves are plotted in Fig. 2. Each element of the coarse mesh is split in four elements in the fine mesh and in 16 elements in the very fine mesh.

In one dimensional computation the internal length can be deduces directly from the values of the parameters. This is less simple for a two dimensional model. in this case, we did some computations of a biaxial test with the same model and the same parameters as the one used in this paper, and we found that the localized zones are 0.25 m. width. In Fig. 3 the areas which correspond to elements smaller that the width of the band are colored for the three meshes showing clearly that the computations discussed in the following are meaningful.

Table 3
Detection of loss of symmetry (P/P_0).

Mesh	Loss of symmetry	Occurrence of elastic unloading
Coarse	16% inc 22	14.5% inc 24
Fine	20% inc 21	18.998% inc 25
Very fine	18% inc 22	16.996% inc 24

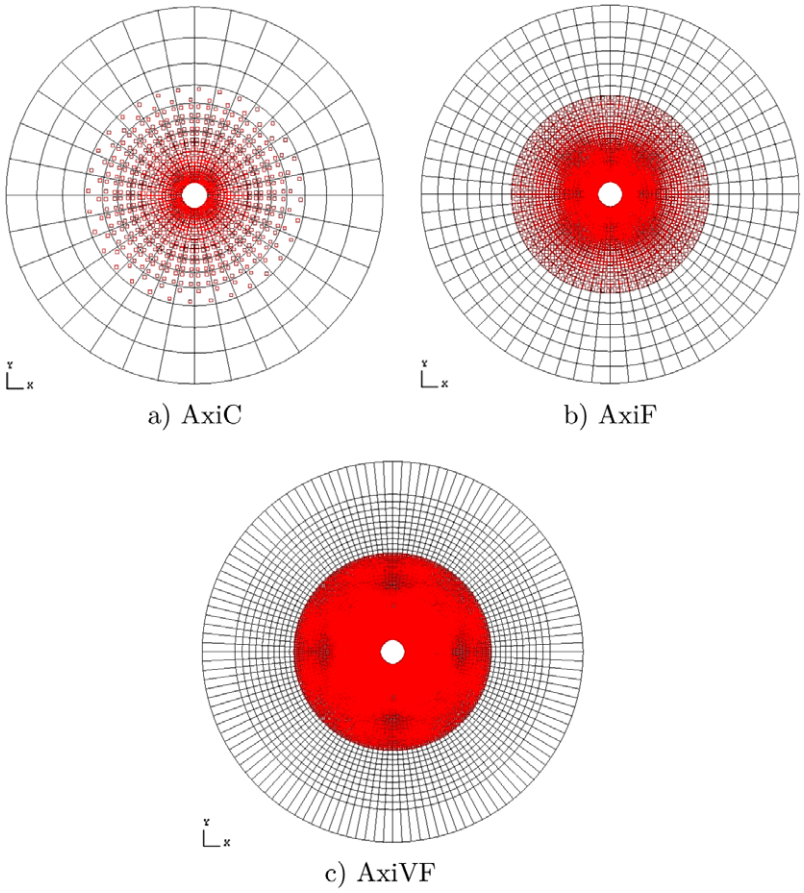

Fig. 7. Plastic loading index for the axisymmetrical solutions (end of the computation).

3.4. Numerical parameters of the computations and description of output data

In the case of non uniqueness, our experience (see Chambon et al. (2001b) for classical computations and Bésuelle et al. (2006) for computations with enhanced model for instance) is that small changes in *numerical data* are able to yield different solutions. Clearly a change of mesh is a numerical data. Consequently it is not so easy to retrieve the same solutions with different meshes. An other numerical datum is the size of the time step. The finite element code used for the numerical experiments described in the following (namely the Lagamine code Charlier, 1987) allows the user to prescribe only the maximum value of the time step. Automatic rescaling of the time step according to the convergence rate of the iterations are done by the code. The following computations have been performed with different

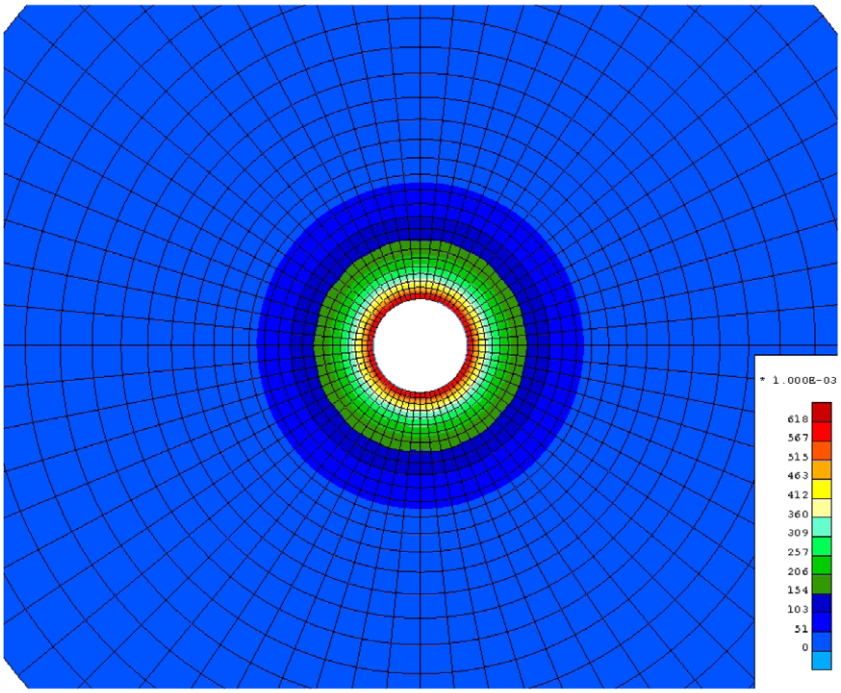

a) Step 20 ($P/P_0 = 24\%$)

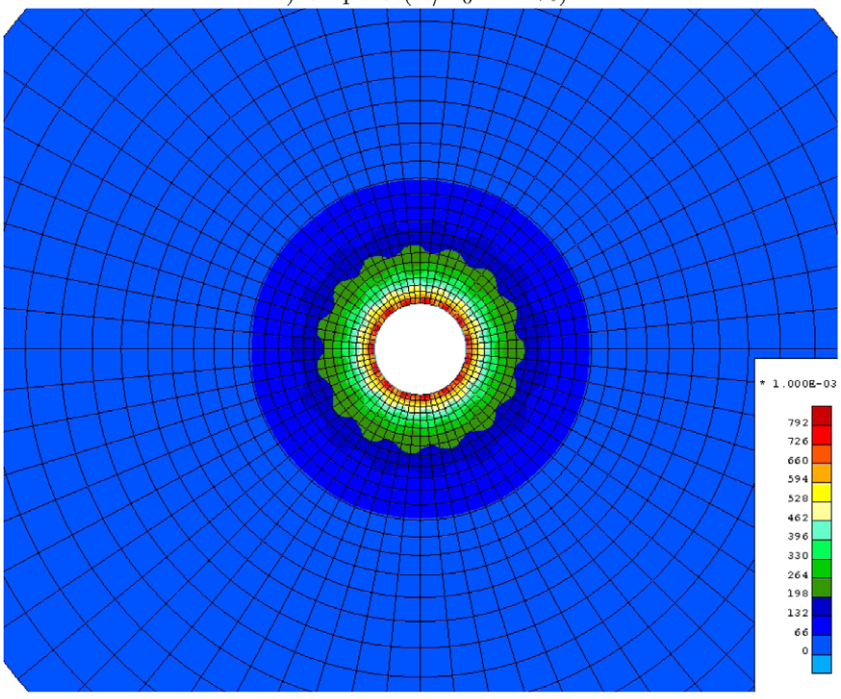

b) Step 21 ($P/P_0 = 20\%$)

Fig. 8. Increment of second strain invariant for BandF11.

meshes and in some case with mechanical defects, but also with different maximum of the time step. For the different computations the input value of this maximum is mentioned in Table 2.

In some cases the initial guess used in the full Newton method for a given time step can be also different according to the method proposed by Chambon et al. (2001b). For some numerical experiments, a random initialization of the initial guess of the Newton method has been used for some time step. If this is the case, the confining pressure for which such a method has been used is mentioned in Table 2.

Visualization of the different solutions is performed by observing the second invariant of the total strain and the loading index or in some case its incremental variation for a given time step. The values of the second invariant of the (total) strain are obtained by interpolating the values obtained in every Gauss point (here we use four Gauss points per element). The loading index of a

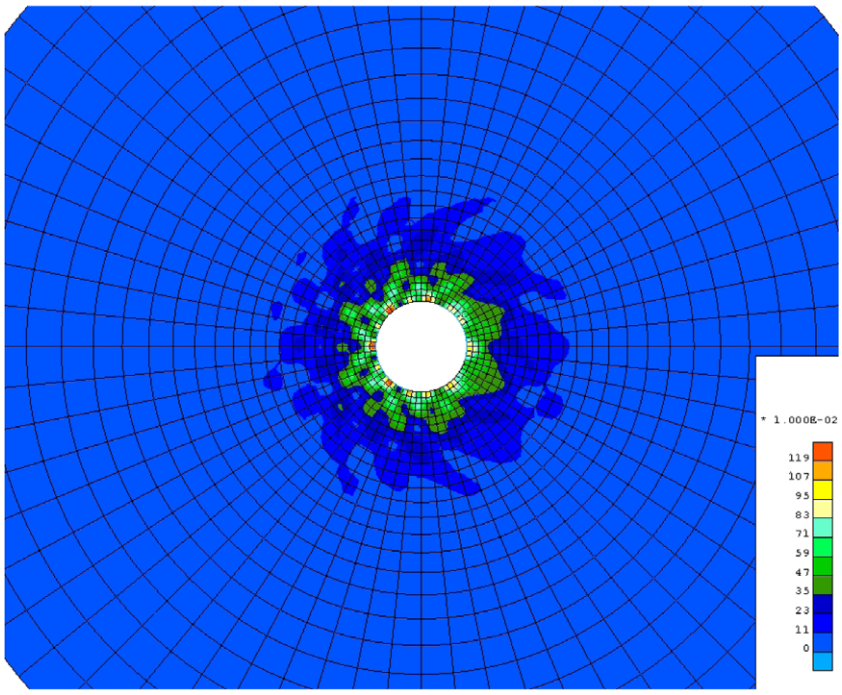

c) Step 24 ($P/P_0 = 19\%$)

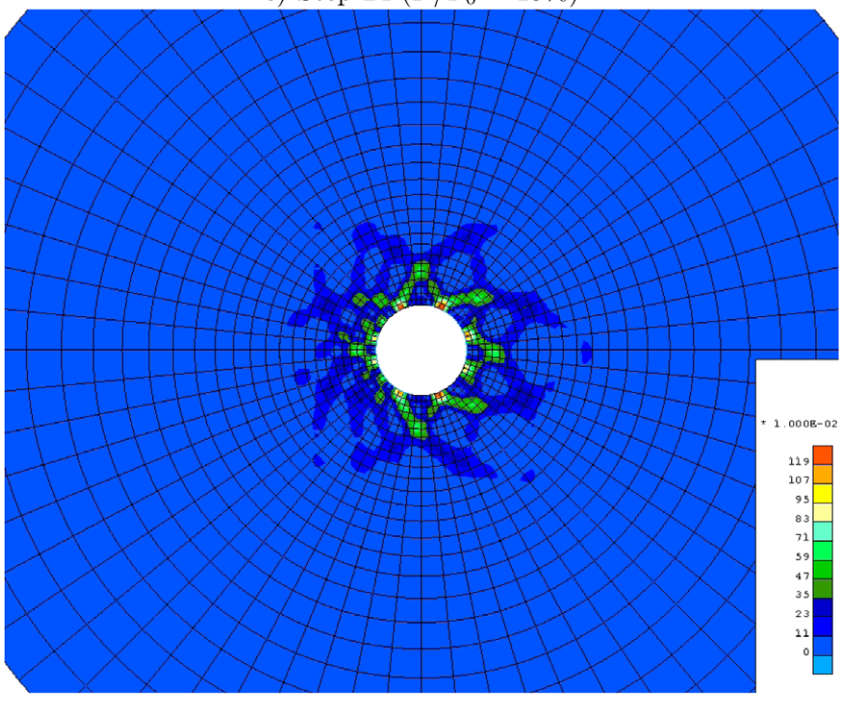

d) Step 25 ($P/P_0 = 18.998\%$)

Fig. 8 (*continued*)

Gauss point for a given time step is defined as follows. When a Gauss point undergoes a plastic loading, then a small square is plotted, otherwise which means that the corresponding Gauss point undergoes either elastic unloading or reloading, in this case, no tag is put on the picture.

The input data of 19 different computations are detailed in Table 2. Other computations have been performed and will be quoted in the comment when necessary. Since they did not produce results different from the ones of the detailed computations, they are not described in Table 2.

4. Axisymmetrical solutions

It is not easy to obtain a prescribed solutions, since as above mentioned small changes in the input data yield different solutions. As already discussed in Section 3.3 the studied problem

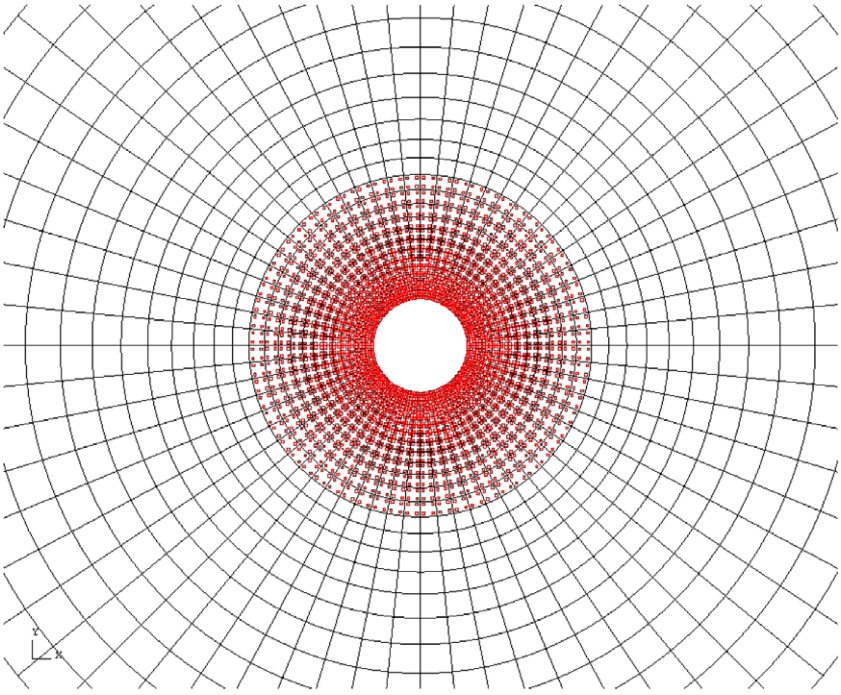

a) Step 20 ($P/P_0 = 24\%$)

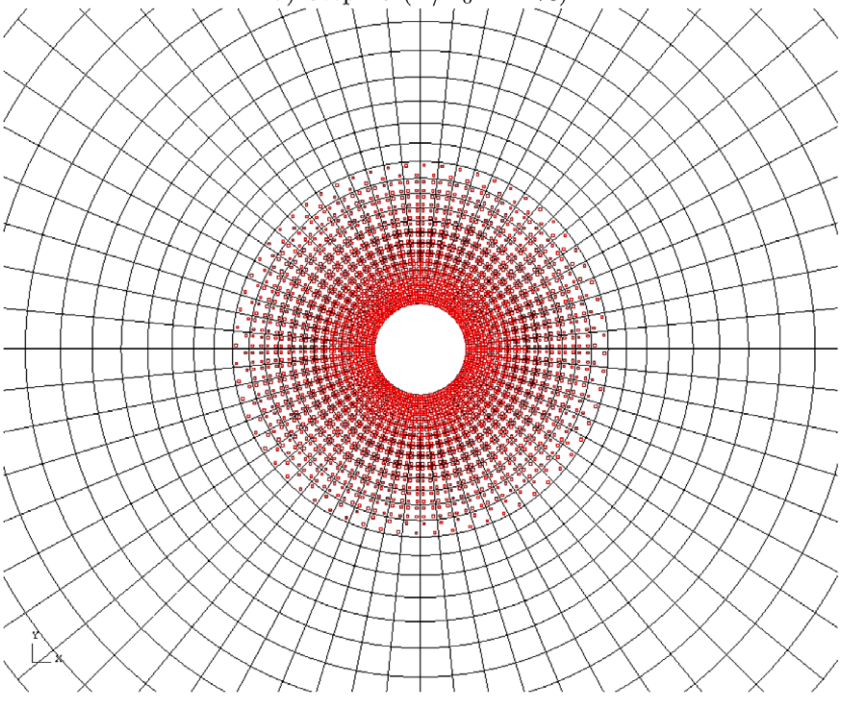

b) Step 21 ($P/P_0 = 20\%$)

Fig. 9. Plastic loading index for BandF11.

has necessarily an axisymmetrical solution. In order to check once more the objectivity of the solutions obtained with a second gradient model, we first try to retrieve the axisymmetrical solution with the different meshes. It is our experience that in order to obtain such a result a large maximum time step is needed. This is clear by inspecting the results depicted in Table 2. It seems that the more symmetric results are obtain with the bigger time steps. This has been already observed in results mentioned by Chambon et al. (2001b) for a plastic buckling problem. However this is only a tendency since the computation named BandC8 (see Table 2) does not meet this heuristic rule.

Fig. 4 shows the loading curves for the first three computations of Table 2. It is clear that the three solutions obtained with the three different meshes coincide. Similarly in Fig. 5 the final radial displacement of a given radius is plotted as a function of the distance to the center of the borehole. Once more the results of the three computations coincide. Figs. 6 and 7 show respectively the final values of the second invariant of the strain and the loading

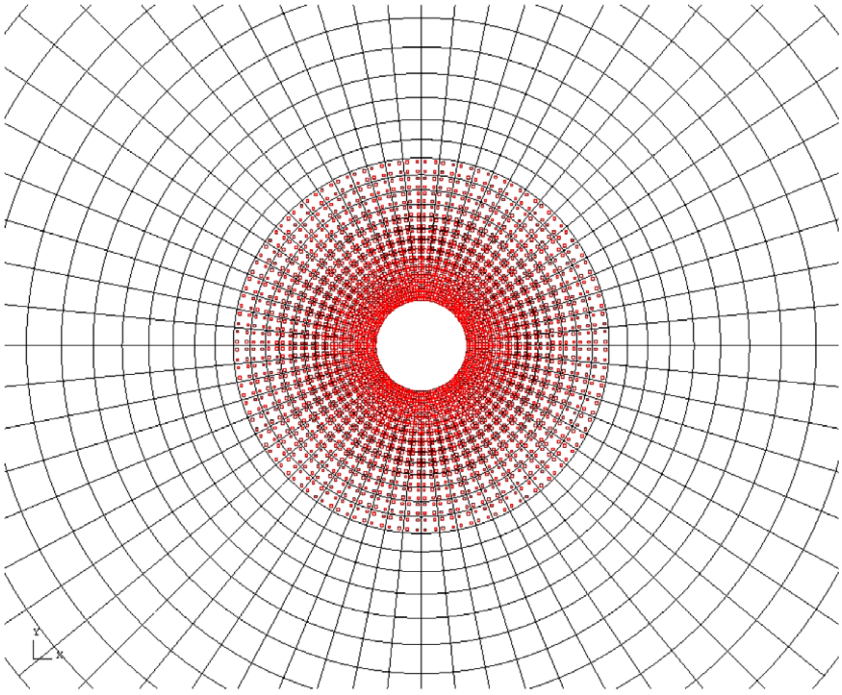

c) Step 24 ($P/P_0 = 19\%$)

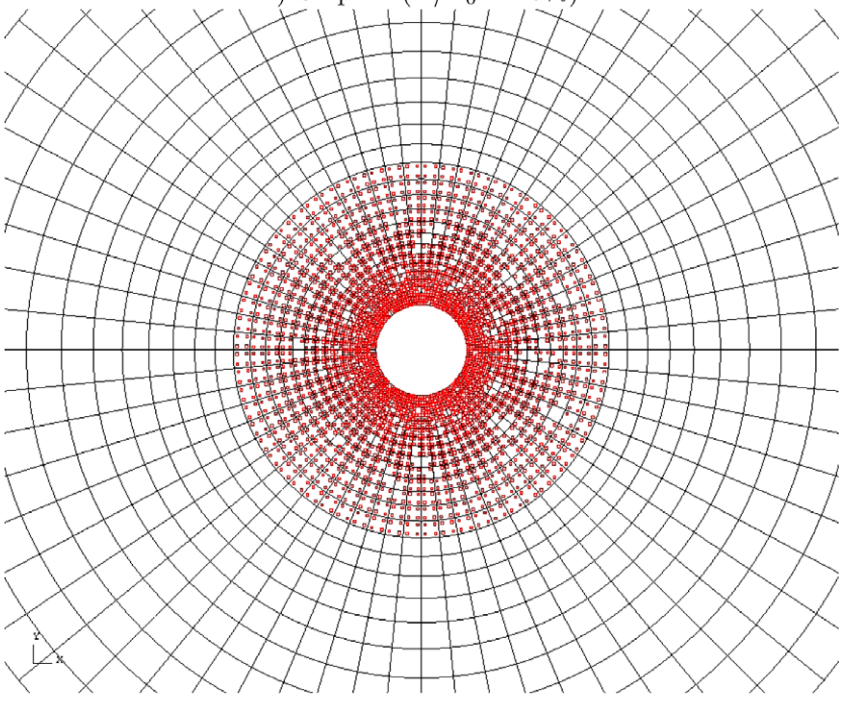

d) Step 25 ($P/P_0 = 18.998\%$)

Fig. 9 (*continued*)

index as defined in Section 3.4. The three final states are the same. The small differences observed can be completely explained by the different interpolations used in order to obtain the pictures.

The three computations behave in the same manner. The beginning of the softening regime starts for the inner layer of elements and the softening area propagates towards the external boundary. At the end of the loading the (softening) plastic zones are the same and the maximum values of the second strain invariant are the same. Very slight differences appear however which make sense with respect to the mesh refinement. Clearly the finer the mesh, the sooner the plastic loading appears. The finer the mesh, the higher the final value of the second strain invariant is. Finally these three computations demonstrate once more the objectivity of the computations with enhanced model provided we are sure to consider the same solution. As seen in the following, the latter condition is questionable in the case of possible bifurcations.

Let us emphasize once more that the parameters used are not the ones of a given rock and consequently neither the bandwidth

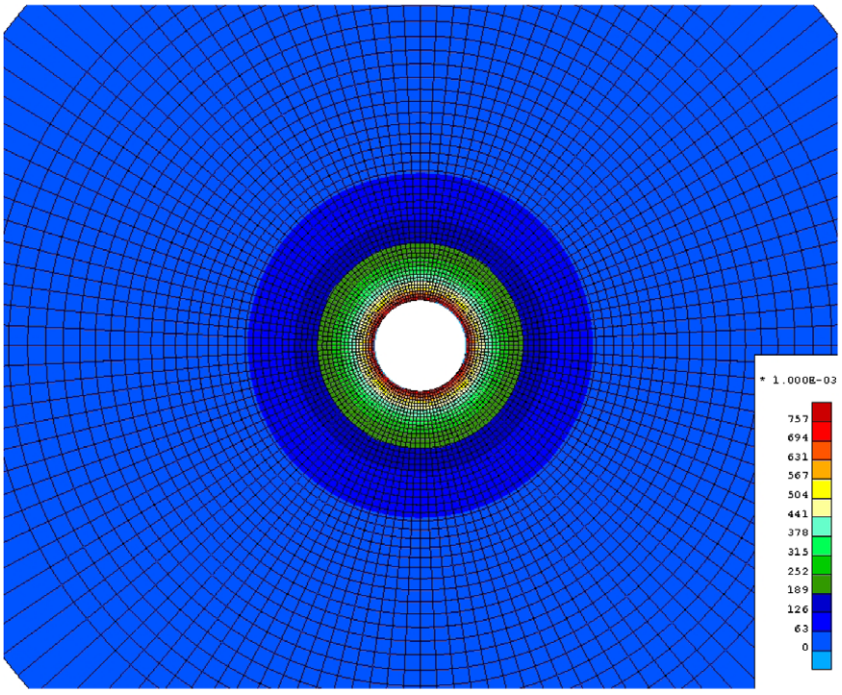

a) Step 21 ($P/P_0 = 20\%$)

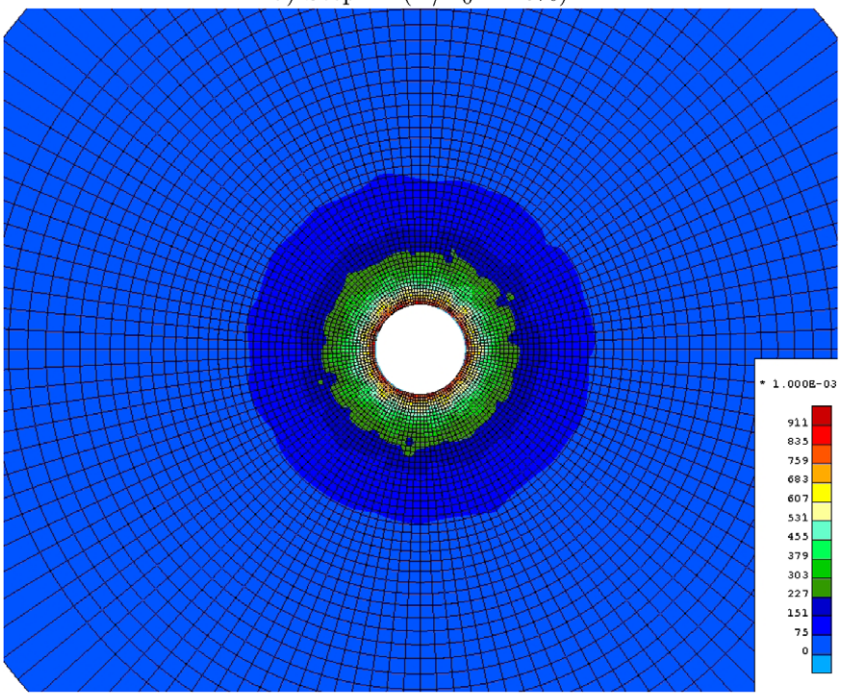

b) Step 22 ($P/P_0 = 18\%$)

Fig. 10. Increment of second strain invariant for BandVF11.

nor the radial displacements of the borehole wall can be compared with in situ measurements.

5. Numerical experiments involving localized areas

5.1. Solutions exhibiting periodic bands in the ultimate state

Let us detail now the results of the computations named BandC7, BandC8, BandC8bis, BandF11 and BandVF11 (see Table 2) which differ from the previous ones by the maximum time step prescribed.

At the beginning of the loading history, all these computations remain axisymmetric, then for a value of around 18% of the inital pressure the exact value depends of the mesh but also of the input data concerning the step size, (see Table 3) the computations loss spontaneously their symmetry. This loss of symmetry is detailed in Figs. 8 and 9 for computation BandF11 and in Figs. 10 and 11 for computation BandVF11. Just after the loss of symmetry, some

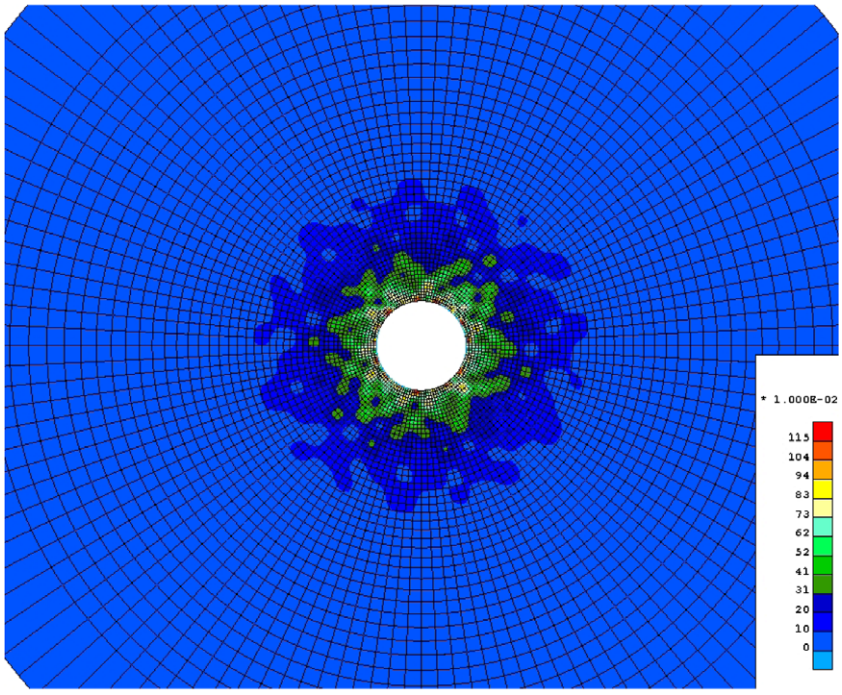

c) Step 23 ($P/P_0 = 17\%$)

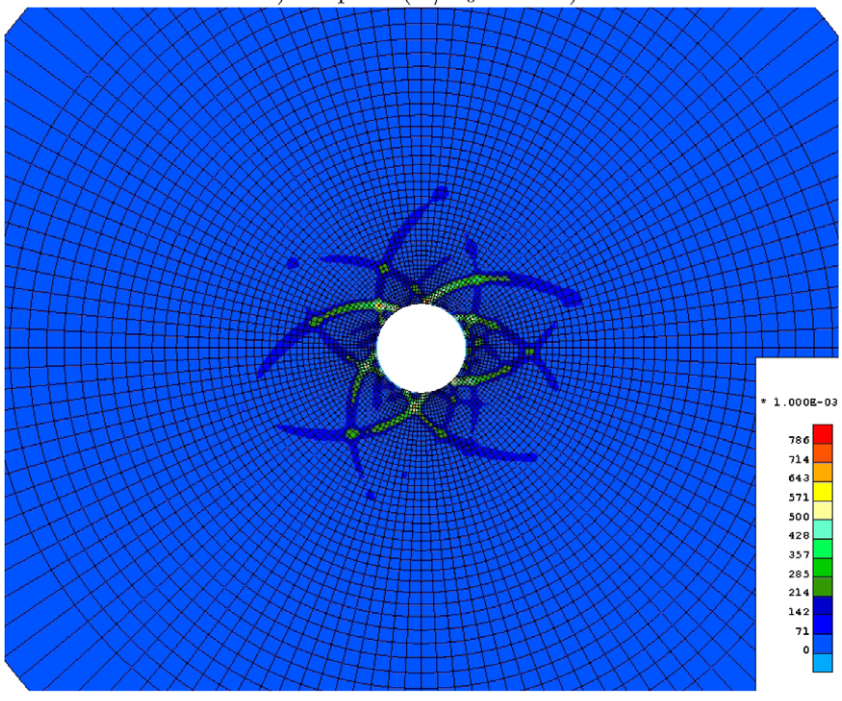

d) Step 24 ($P/P_0 = 16.996\%$)

Fig. 10 (*continued*)

Gauss point unload giving birth to localised bands. This is described in Table 3 where computations with coarse, fine and very fine meshes are compared.

Similarly to what is already mentioned by Chambon et al. (2001b), we observed that convergence is more difficult for the step corresponding to the loss of symmetry. This induces an automatic drastic decreasing of the step size. It is divided by 500 in the case of fine mesh (computation BandF11) and by 250 in the case of very fine mesh (computation BandVF11). As seen in Figs. 8d and 9d for the fine mesh 18 the patterns appearing just after bifurcation exhibit crossing bands. In the case of very fine mesh 23 crossing bands emerge more clearly (see Figs. 10d and 11d).

The corresponding pictures for computations BandC7, BandC8, BandC8bis (coarse mesh) have not been given. They show similar results. However in these cases, even if close to the center, the elements are small enough, as far as the bands propagates toward the external boundary, the size of the elements become more and more large with respect to the almost constant internal length. It

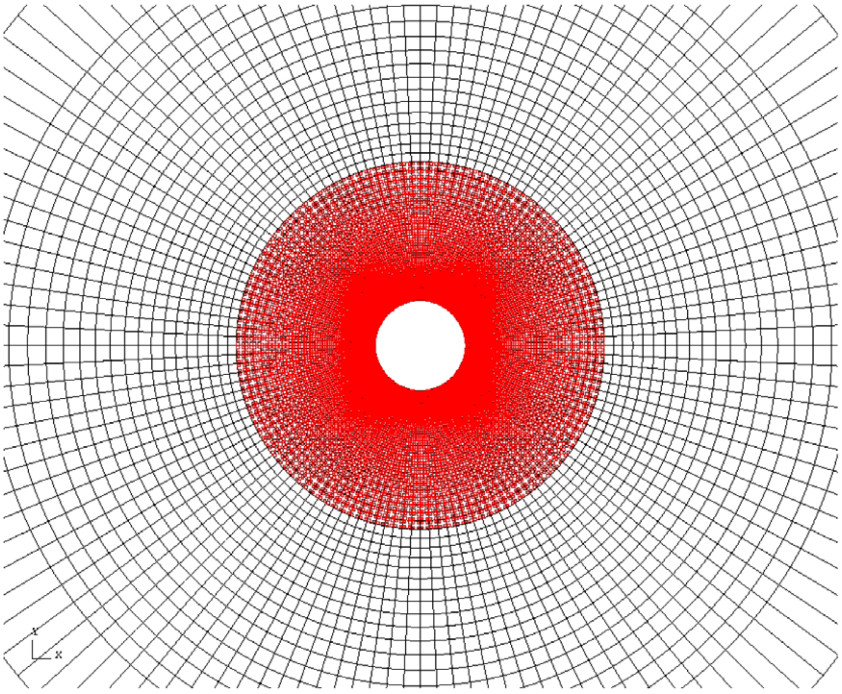

a) Step 21 ($P/P_0 = 20\%$)

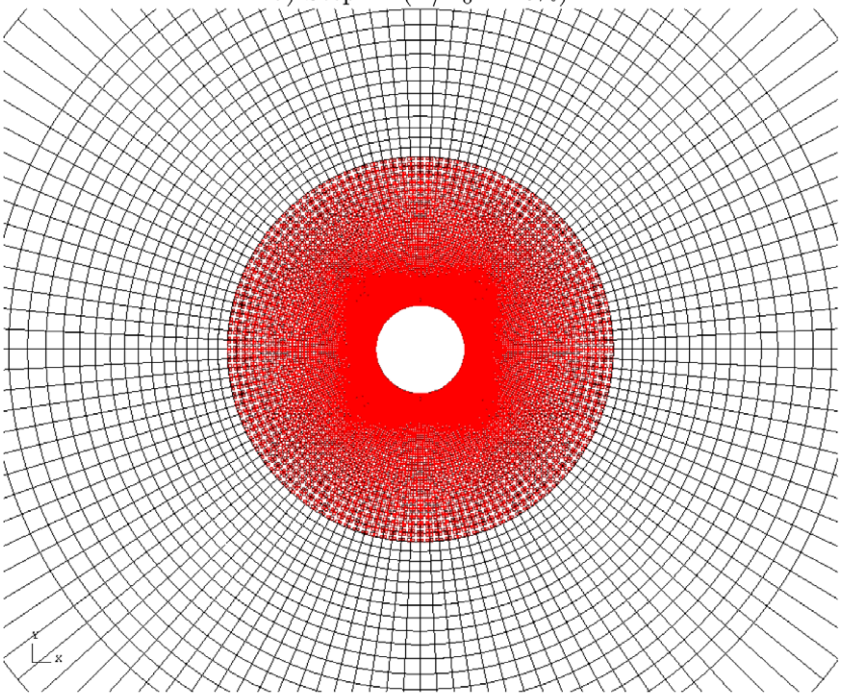

b) Step 22 ($P/P_0 = 18\%$)

Fig. 11. Plastic loading index for BandVF11.

is likely that the mesh is too coarse when the band are fully developed.

Looking once more to Figs. 8 and 10, it seems that localization evolutions follow the scenario found by Vardoulakis and Sulem (1995, Chapter 10,) and by Papanastasiou and Vardoulakis (1992) for Cosserat Continuum. Bifurcations in computations BandC7, BandC8 and BandC8bis not presented in this paper give similar results. Some waves appear in the inner boundary of the problem, expand toward the outer boundary and localize. Let us recall that the analysis done by Vardoulakis and Sulem (1995) is obtained for a linear comparison solid. The number of waves involved in the bifurcation mode is not unique and depends on the computation. But it is clear that the order of magnitude of this number is related to the internal length. The ratio between the circumference of the inner wall of the borehole and the internal length is around 13 which is consistent with the observations of the numerical

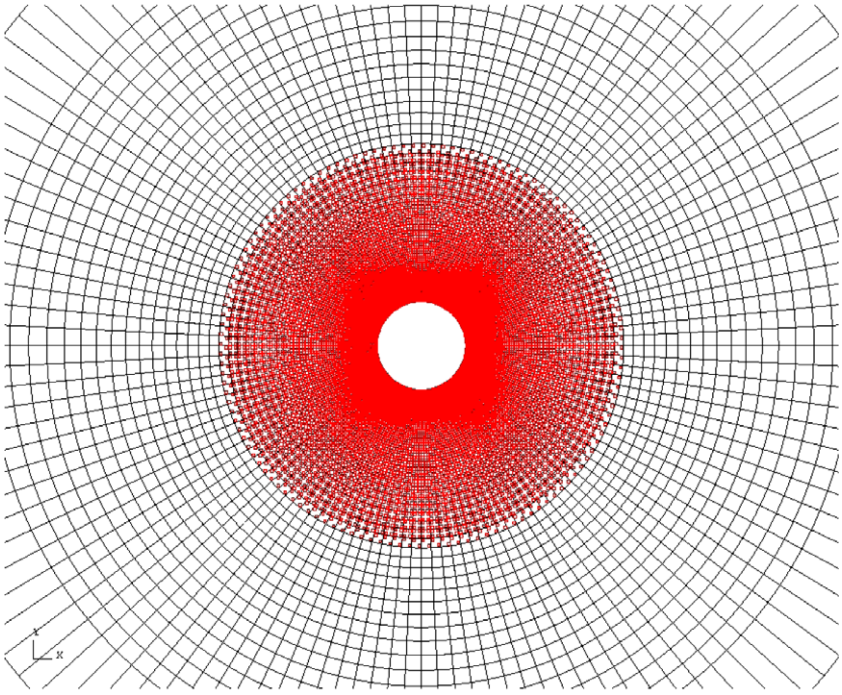

c) Step 23 ($P/P_0 = 17\%$)

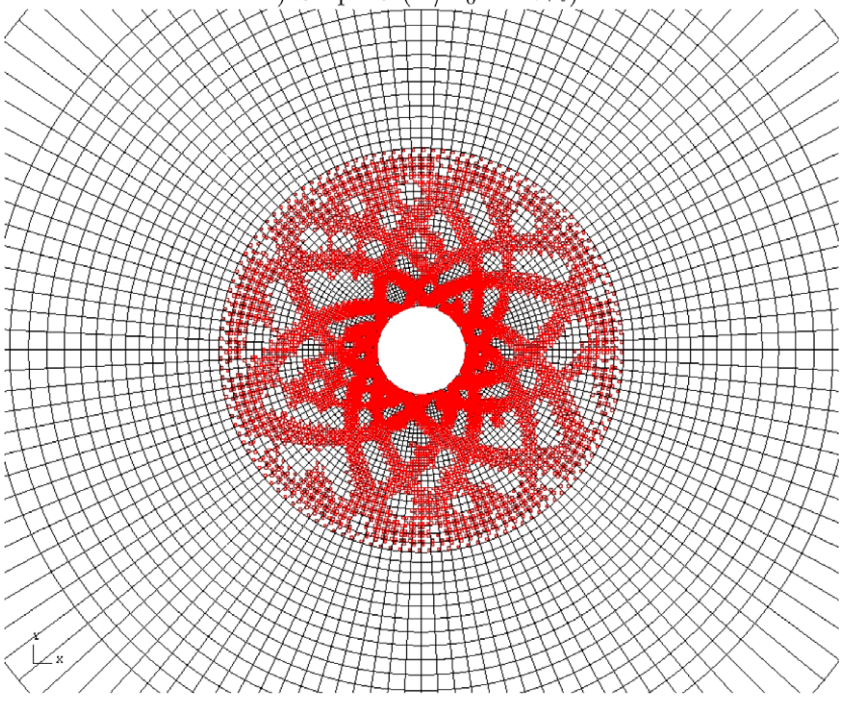

d) Step 24 ($P/P_0 = 16.996\%$)

Fig. 11 (*continued*)

computations. The non uniqueness of the wave number is similar to what has been observed in one dimensional problem by Chambon et al. (1998).

Figs. 12–14 show the final state of computations BandF11 and BandVF11. The two final states appear to be similar. Eleven spiral like bands are active at the end of the loading history. The widths of the band are the same and independent of the mesh size. However with respect to an initial boundary value problem the solutions are not the same. This is obvious by comparing Figs. 8 and 10 on one hand and Figs. 9 and 11 on the other hand. The routes going to the similar final solutions are clearly not identical.

The large values of the second strain invariant observed in some points of the localized zones at the end of the computations are probably unrealistic. They are partly due to the extrapolation procedure used in order to obtain the pictures. Clearly in this case the use of a hypoelasto-plastic model is questionable. It should be better to use a hyperelasto-plastic second gradient model like the one

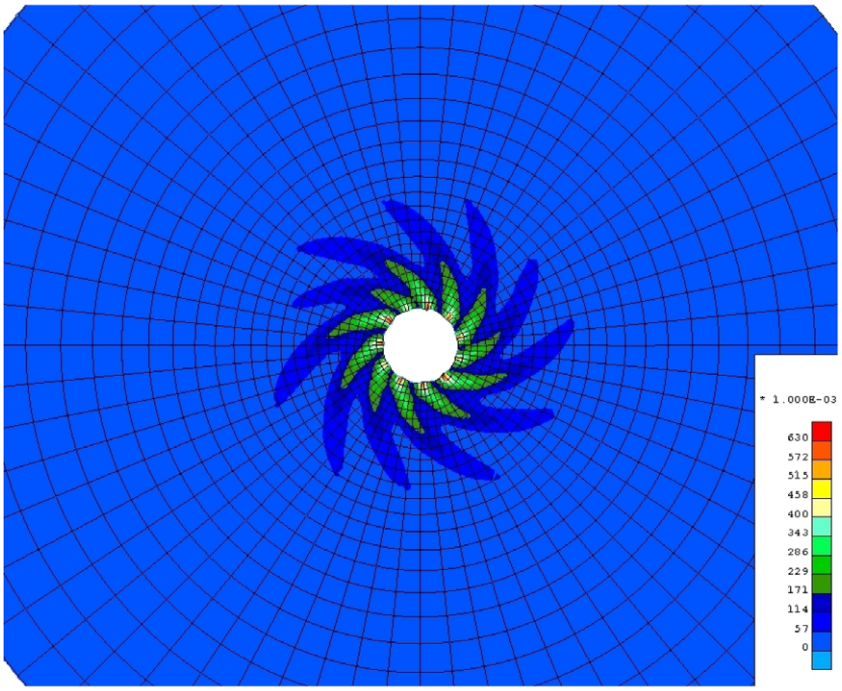

a) BandF11

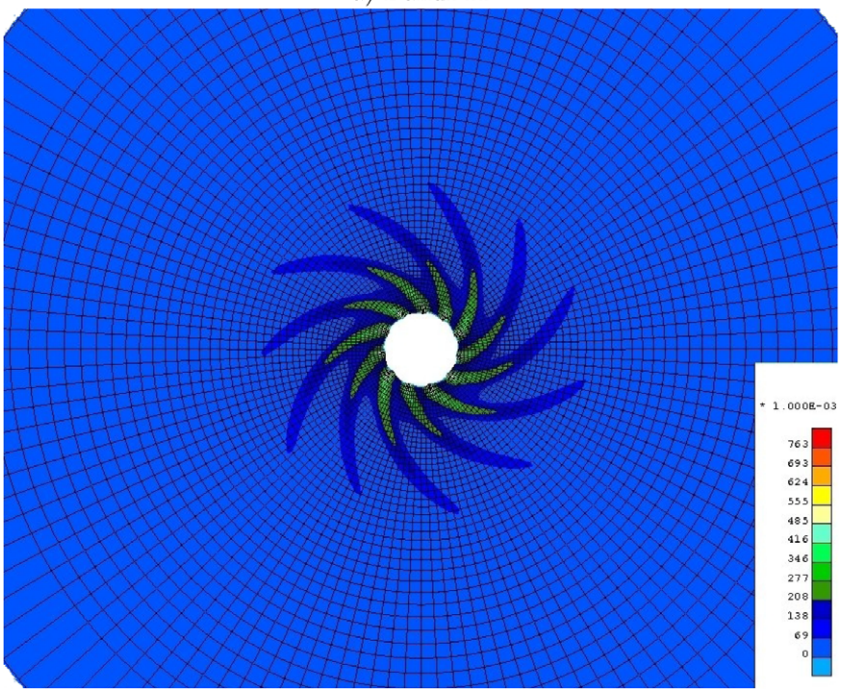

b) BandVF11

Fig. 12. Final values of the second strain invariant.

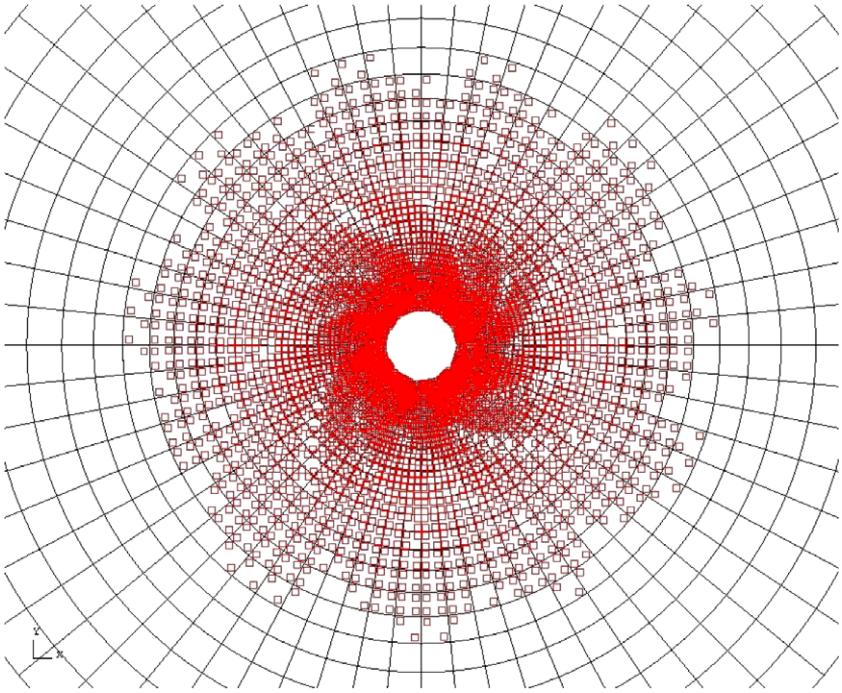

a) BandF11

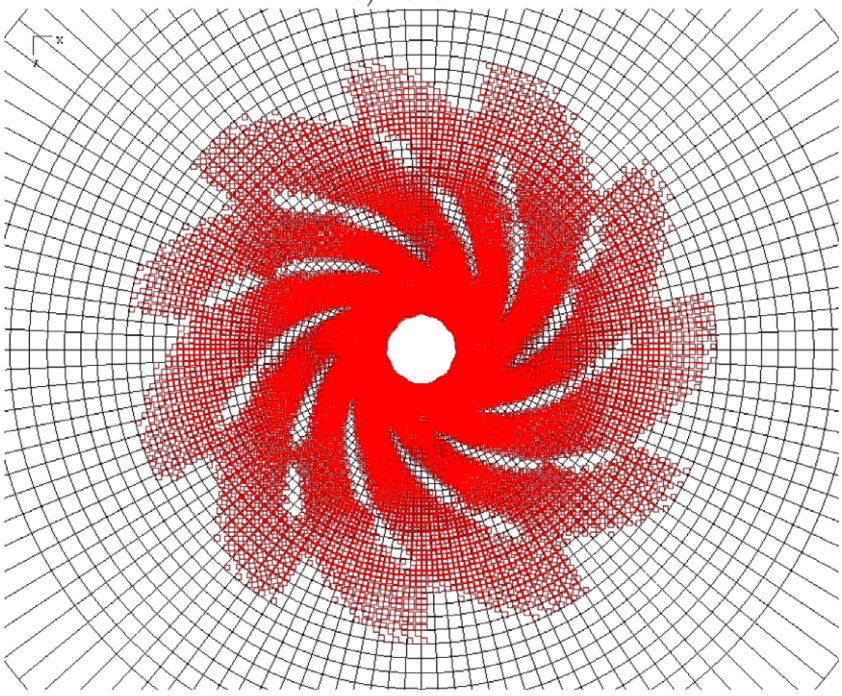

b) BandVF11

Fig. 13. Final plastic loading index.

developed by Chambon et al. (2004), which unfortunately has not yet been used in computations.

Finally in Fig. 15 the internal pressure is plotted as a function of the average radial displacement for the three different mesh sizes. From a mechanical point of view the three computations behave in a similar manner and in fact quite close to the corresponding results obtained for axisymmetric solutions (see Fig. 4). However for phenomena for which the details of the localized zones are important the different solutions have to be seen as rather different. This can be important if we want to model hydro mechanical coupled behavior. In this case the degradation of the materials in the localized zone can induce drastic changes in the permeability of the media and consequently of the transmissivity of the borehole. Fig. 16 shows the radial displacement of points of a given radius at the end of the loading as a function of the distance to the center. Once more the different curves are close together, but since the positions of the localized bands are not the same, some fluctuations, different from one solution to the other, appear clearly.

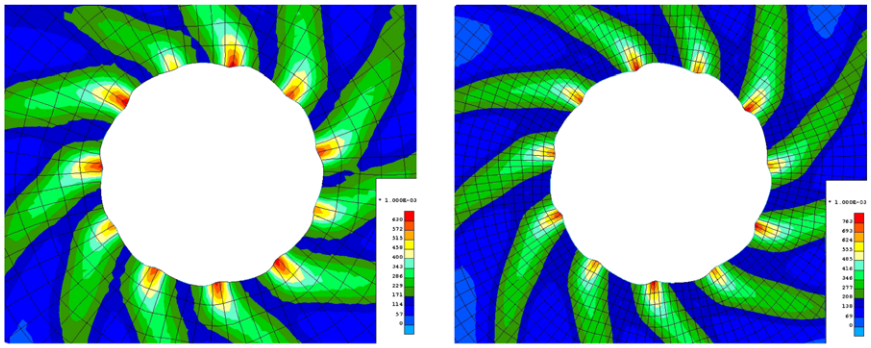

Fig. 14. Final values of the second strain invariant: zoom.

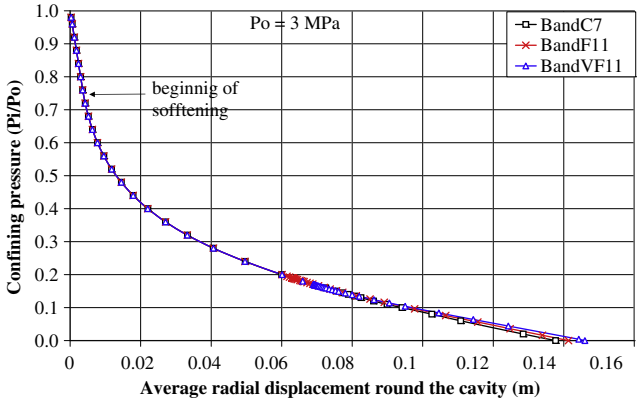

Fig. 15. Internal pressure as a function of the average radial displacement.

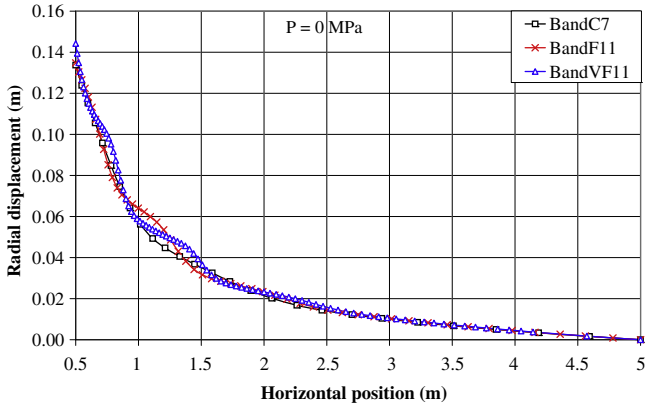

Fig. 16. Radial displacement of a radius at the end of loading as a function of the distance to the center.

5.2. Other localized solutions

In this section two different techniques are used in order to find other solutions. Computations BandVF12, CrossF and CrossVF differ only from the previous ones by the input numerical data, the observed patterns occur spontaneously. The method first proposed by Chambon et al. (2001b) consisting in starting the Newton iterations of a given time step with some random guess is used for computations BandF10 and BandF10bis. Both methods yield other solutions than the ones detailed in the previous section.

Fig. 17 shows the final state of the three computations performed with the fine mesh. Clearly this demonstrates the non uniqueness of the solutions of the studied problem. Not only the number of spiral like bands can differ (since now a solution with 10 bands can be observed), but instead of a pattern of spiral bands another pattern can emerge from the computation, where localized bands cross each other.

Fig. 18 shows two other solutions with the very fine mesh confirming that another pattern of localized band is a suitable solution. Computations with a perfect (perfect means here without intentional defect) numerical model demonstrate clearly the loss of uniqueness of the solution of the problem studied so far. Moreover theoretical considerations can proved that there are many other solutions. All the solutions found can be rotate with an arbitrary angle, they also can be transformed through an arbitrary symmetry. Moreover it is easy to find other solutions for instance by computing half of the domain with proper symmetry boundary conditions. A quarter of the domain should also give other solutions. Finally it is quite clear that the problem undergoes a big number of *different* available solutions (different means here considering as only one solution all the solutions obtained by symmetries or rotations starting from the same solution).

5.3. Solutions obtained with a weak area

It is often believed that uniqueness of solutions is restored by introducing some *physical* defect in a computation. This point is studied in the present section. In order to be sure to compute the same problem with three different meshes a defect is introduced is a small area of one element in the coarse mesh corresponding to four elements in the fine mesh and to 16 elements in the very fine mesh. The defect is a reduction of 5% of the value of the parameter e_{lim} for the material of this area. This area appears in grey in all the following figures. In order to study once more the uniqueness of solutions, the three computations are performed twice but with different time steps (see Table 2).

Figs. 19 and 20 show the final states of two solutions obtained with the fine and the very fine mesh. Inspecting these figures reveals that in fact one solution is obtained from the other by a symmetry. On the other hand Figs. 21 and 22 show clearly that a defect does not restore uniqueness since the two solutions corresponding both to a spiral like pattern involve a different number of bands.

6. Concluding remarks

Loss of uniqueness of numerical solutions of a problem less simple than the ones obtained by modeling element tests has been clearly demonstrated. This result has been obtained for a second

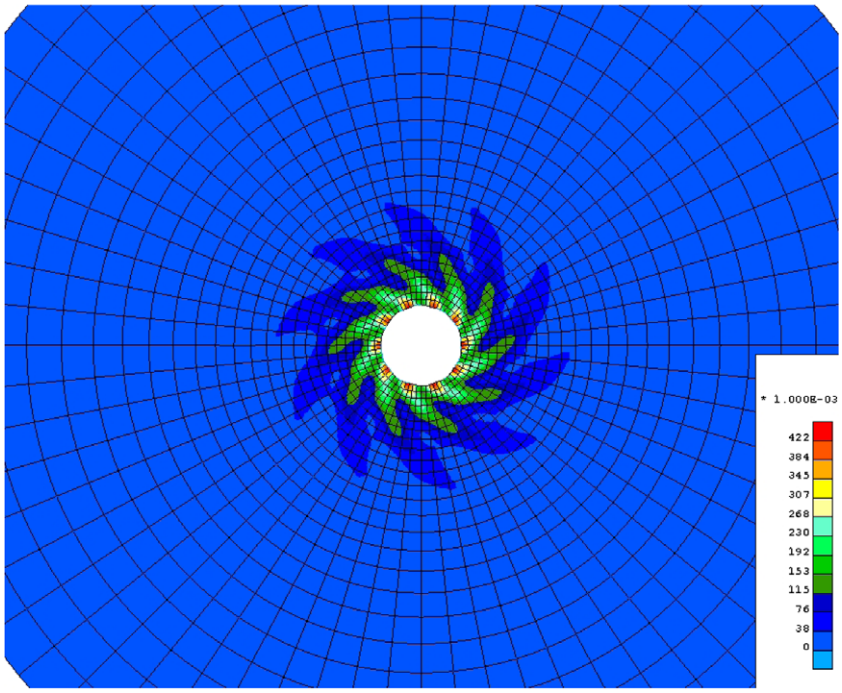

a) BandF10

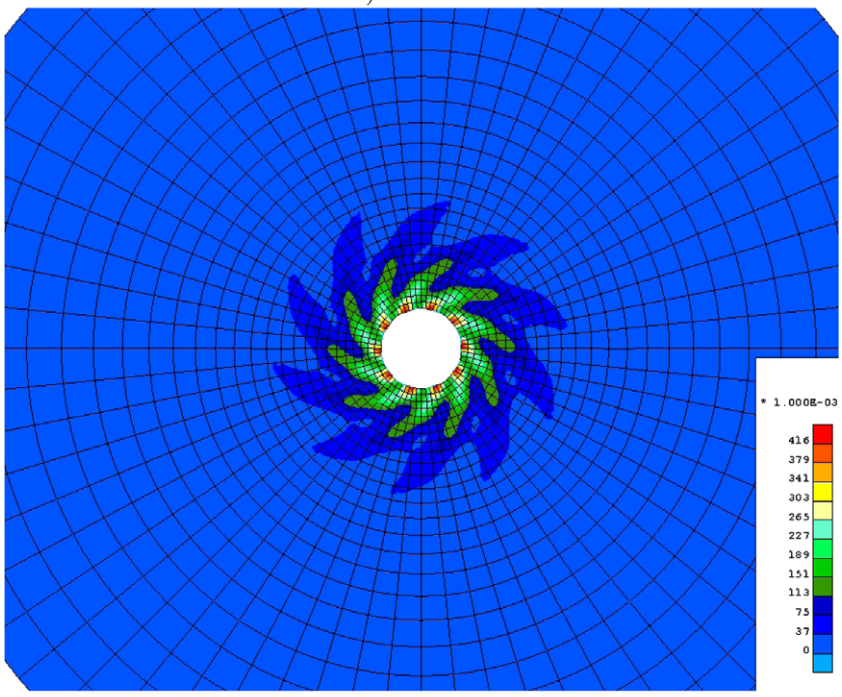

b) BandF10bis

Fig. 17. Final values of the second invariant of the strain: other solutions with the fine mesh.

gradient model, i.e. a model incorporating an internal length. It is necessary to consider these results when performing computations. A nice convergence towards a solution for every time step of a computation is not at all a proof of having found an approached solution of the assumed (unique) solution. Consequently, especially for difficult problems, it is useful to duplicate computing by changing input numerical data such as the mesh size, the time step size and even the initial guess of the Newton method used to solve the non linear equations of every time step. It would be good to have mathematical results indicating the existence and uniqueness of the solution of the underlying mathematical problem and of the corresponding numerical problem. Similarly convergence results proving that by refining the spatial and time dicretizations, numerical solutions approach the solution (or the solutions) of the underlying mathematical problem should be very interesting. Unfortunately such proofs are lacking. Therefore the following remarks have to be considered only as possible interpretations of the results presented in this paper.

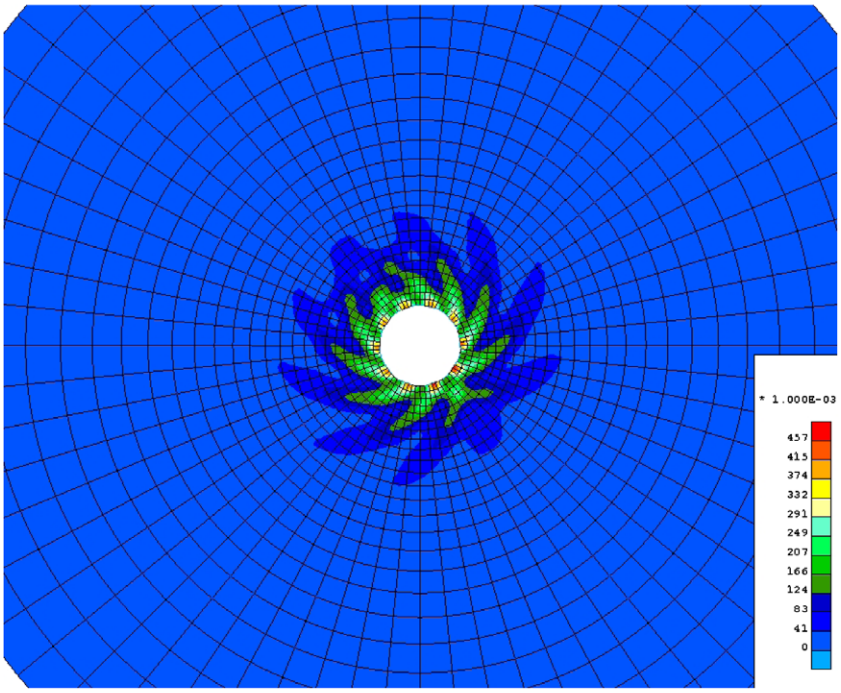

c) CrosF

Fig. 17 (*continued*)

For the one dimensional computations reported in Chambon et al. (1998), it is possible to exhibit all the solutions of the problem, which means that, in this restricted case, the mathematical problem is well understood. In this case, the corresponding numerical computations are able to provide approximate solutions for every solution of the underlying mathematical problem. It is therefore likely that we are in a similar situation for the numerical computations reported in this paper. The studied borehole problem may have several solutions, and for some of them corresponding numerical solutions are found.

In reality, only one solution can be observed, but we are working on a continuum model of the reality (even if it is an enhanced one), which is not able to take into account all the details. This is usual in engineering. We know that geomaterials are in fact heterogeneous materials, and it can be thought that the observed solution is selected by the details at the micro scale, which are not observable. This view point is corroborated by the few published experimental data. In the computations we detect at least two kinds of localized pattern, multiple spirals pattern and crossing bands. Unfortunately it is not possible to find in the literature experimental results exhibiting both patterns with the same materials. However, in a recent paper, Crook et al. (2003) cite experiments on thick-walled cylinders where both modes are observed, even if they have not been obtained with the same material. For more simple problems (namely modeling a biaxial) the loss of uniqueness of the numerical solutions has been related with the loss of reproducibility of the experimental data (see Bésuelle et al., 2006). It should be the same for the borehole problem. Reproducibility of the experiments on thick wall-cylinder should be done in order to confirm (or not) our way of thinking.

Another issue is that the observed solution is perhaps the only stable one. Clearly a stability analysis should be interesting. A stability study should involve dynamic modeling around the quasi-static solutions in order to choose, among the several quasi-static solutions, the one which is (or the ones which are) stable. Unfortunately such a study is not easy to do even numerically, mainly because a linear stability analysis is not sufficient due to the switch between loading and unloading for many material points of the studied structures. Moreover we model materials undergoing friction and cohesion, and it is our opinion that several solutions are stable.

We think that the non uniqueness of the numerical solution is not related to the particular enhanced model used (namely the second gradient one). In the above mentioned paper of Crook et al. (2003), modeling using the fracture energy regularization is performed which reproduces both modes. The details of the computations are not given in the quoted paper, but it is clear that in order to obtain the crossing bands pattern, only half of the structure is modeled, which is not necessary as proved by our results. We think that the multiplicity of solutions will appear with any enhanced model in every computation for which the classical part of the model exhibits softening.

From an engineering point of view, the loss of uniqueness does not induce necessarily difficulties. It is possible that the details of the solutions are not important with respect to the design of the studied structure.

As a conclusion, the validation of a model done to reproduce the behavior of the degradation of materials should be performed by a comparison of the set of (obviously non unique) numerical solutions with the set of data coming from (wanted) identical experiments. Doing that, we have to keep in mind that the study of the non uniqueness of solutions suffers from three main and presently unavoidable drawbacks. First, if there are a great number of solutions, only some of them are stable with respect to the algorithm used to find them and this stability has nothing to do with the physical stability. Second, it is likely that we do not find all the solutions. Third, the numerical solutions are only projections (in the sense of the functional analysis) of solutions on to a finite dimensional space and in doing that, some solutions can be completely hidden by the numerical procedure. However, in any case we have to face this unpleasant problem of non uniqueness of solutions.

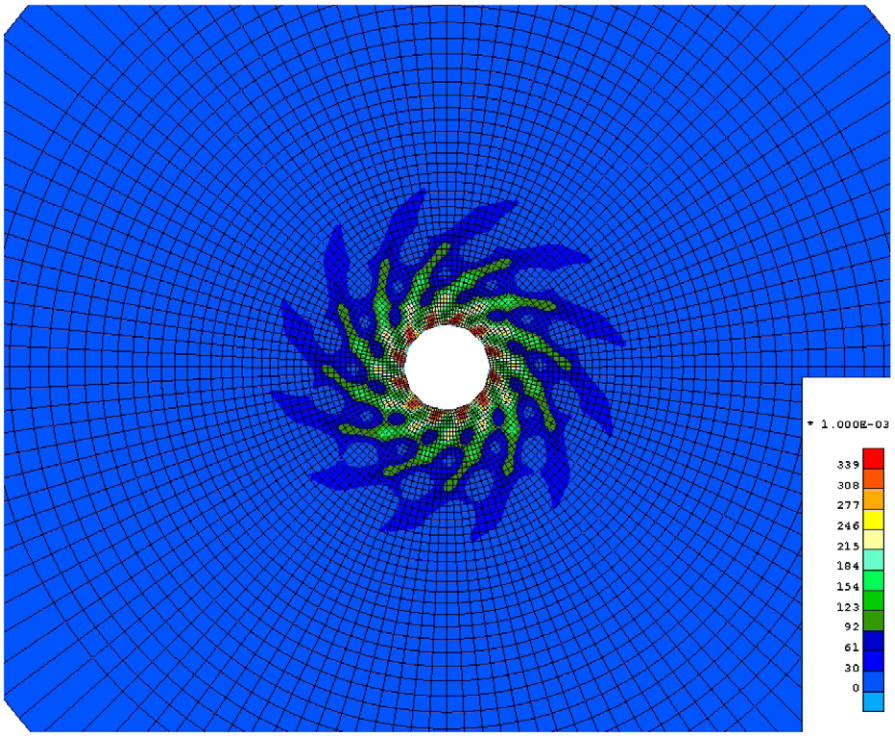

a) BandVF12

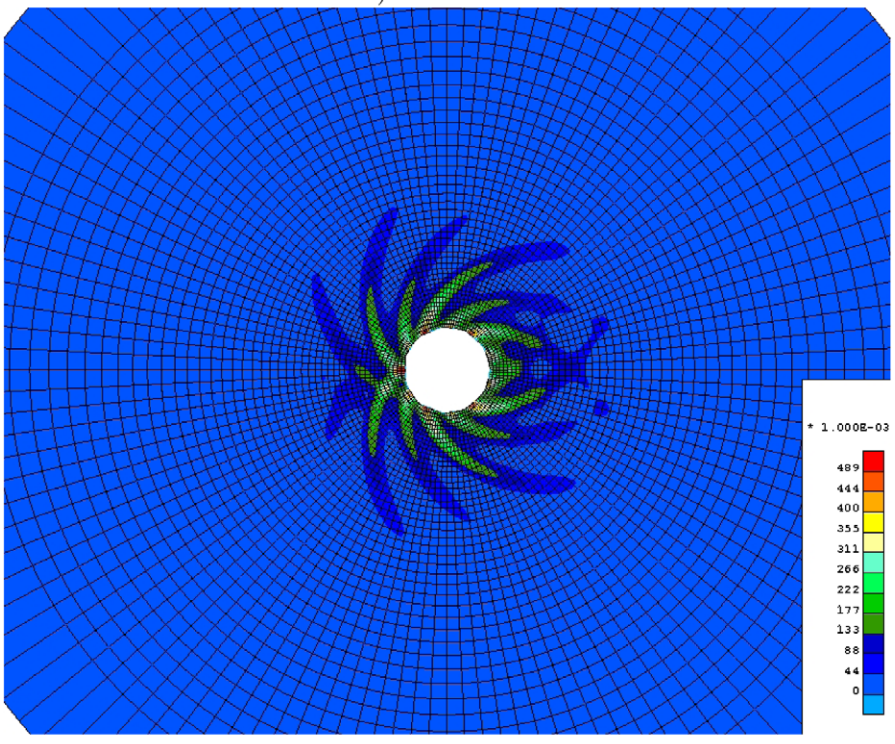

b) CrosVF

Fig. 18. Final values of the second invariant of the strain: other solutions with the very fine mesh.

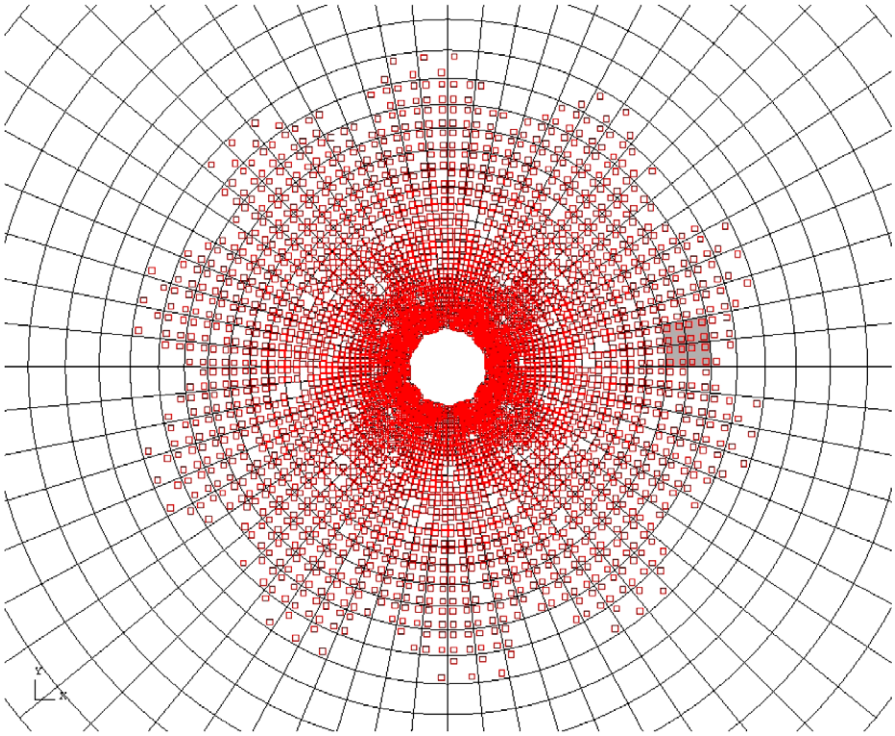

a) WeakF1

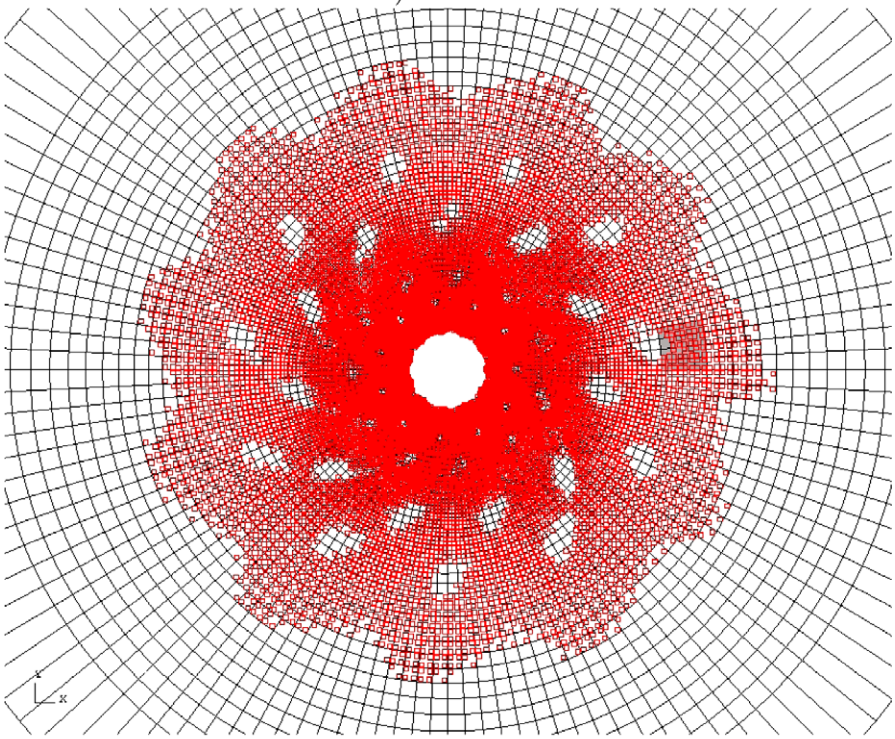

b) WeakVF1

Fig. 19. Final plastic loading index for two computations with a weak area.

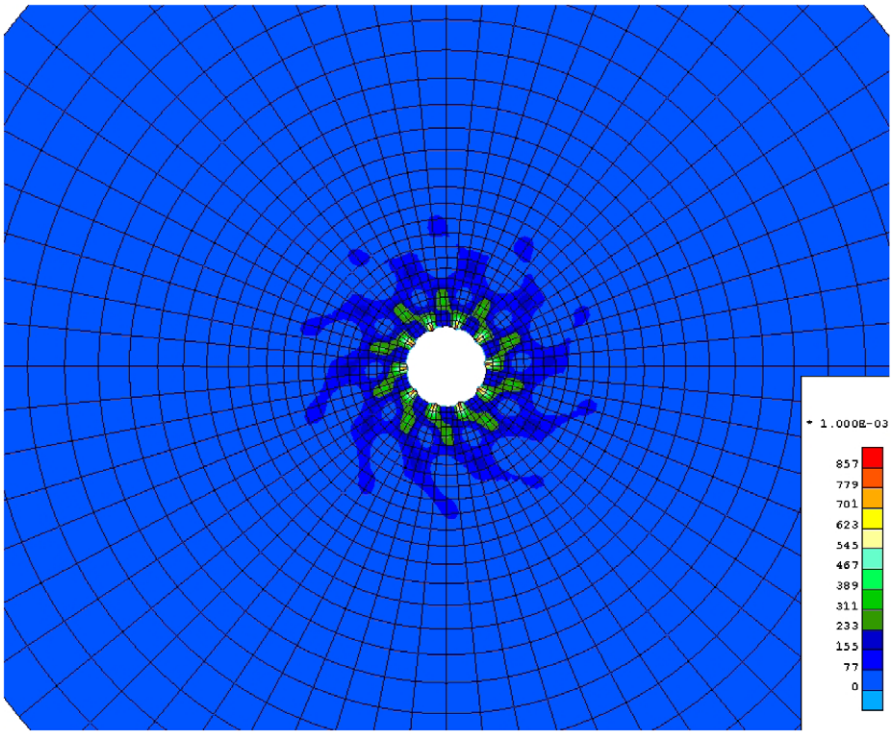

a) WeakF1

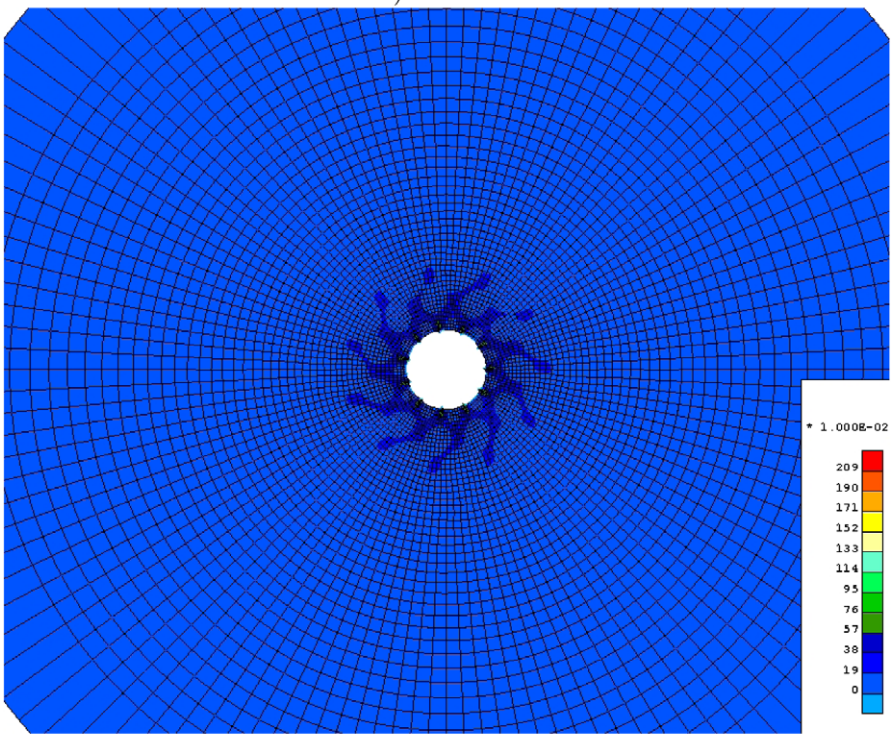

b) WeakVF1

Fig. 20. Final values of the second strain invariant for two computations with a weak area.

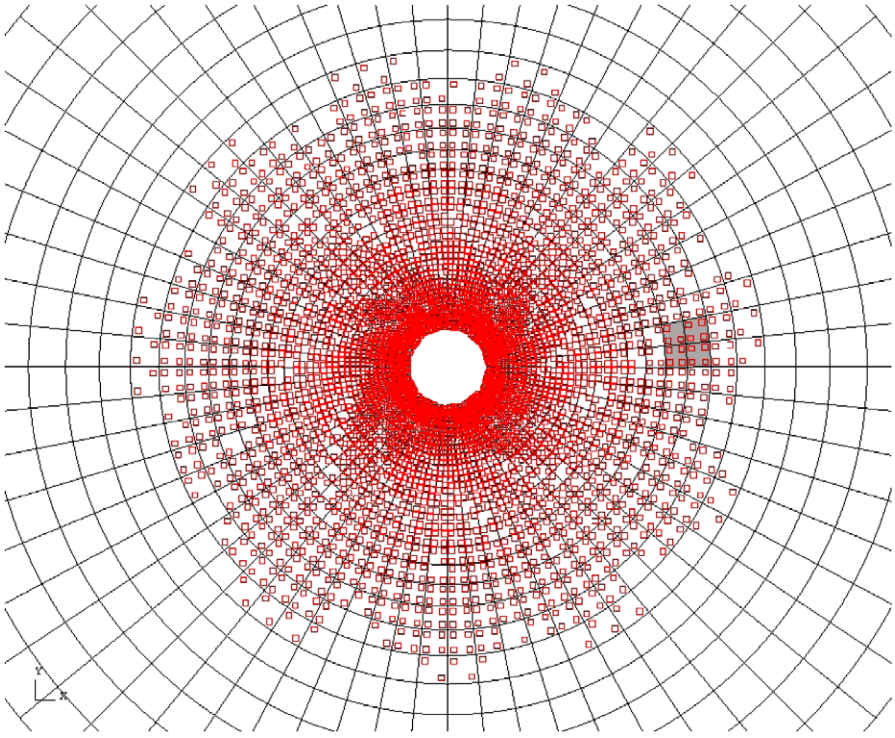

a) WeakF2

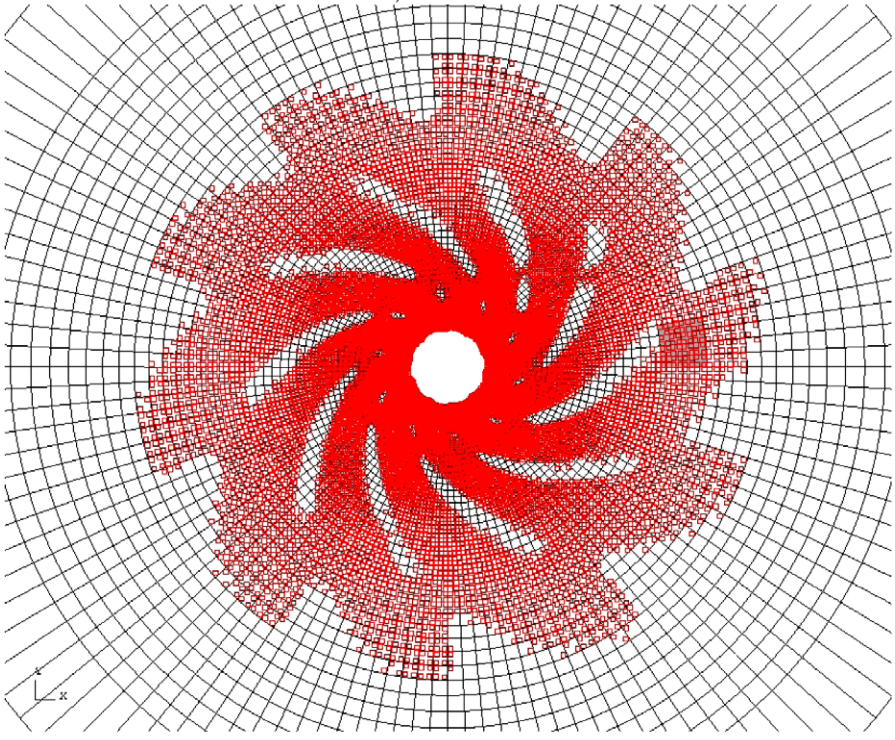

b) WeakVF2

Fig. 21. Final plastic loading index for two other computations with a weak area.

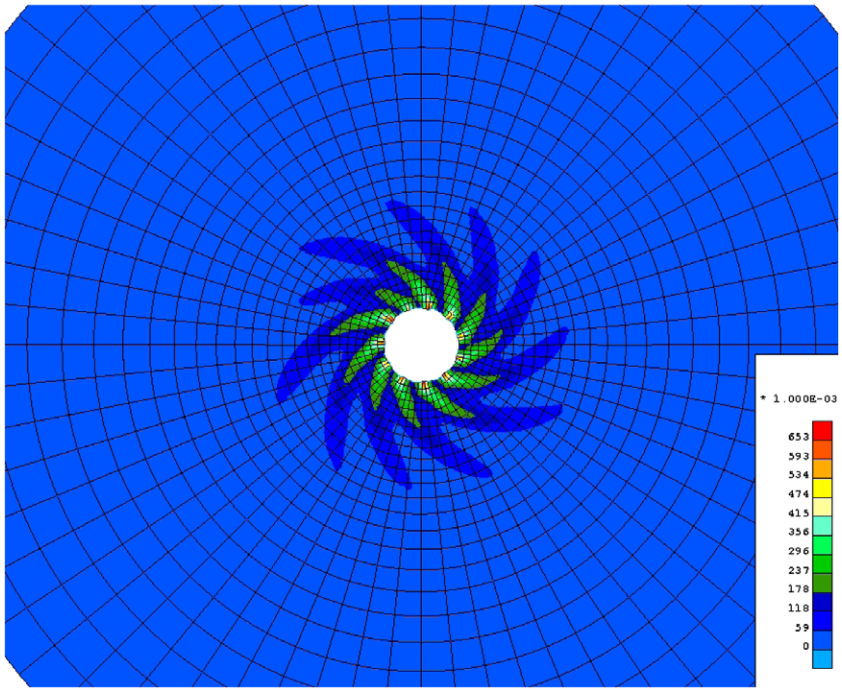

a) WeakF2

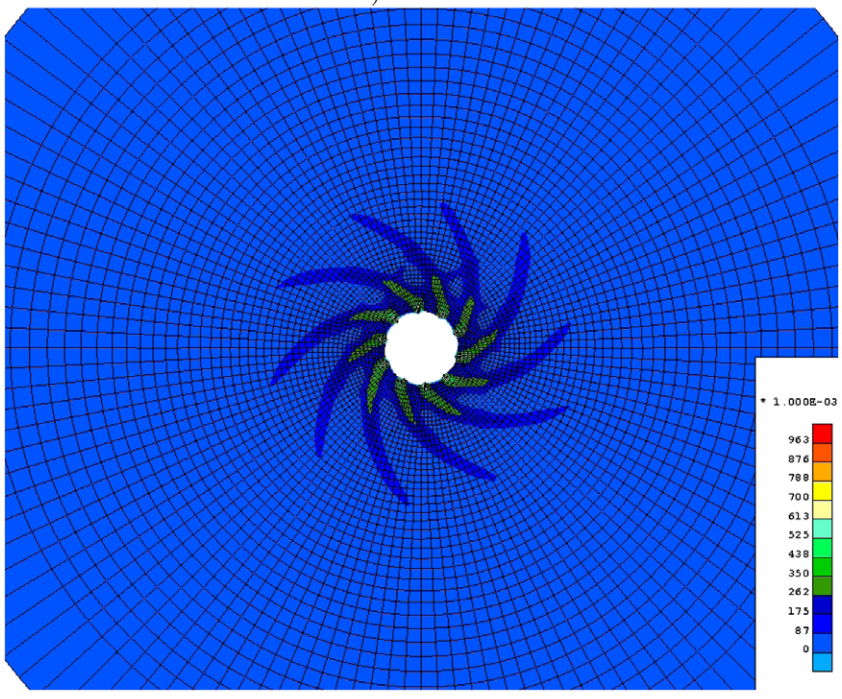

b) WeakVF2

Fig. 22. Final values of the second strain invariant for two other computations with a weak area.

References

Aifantis, E., 1984. On the microstructural origin of certain inelastic models. Journal of Engineering Materials and Technology ASME 106, 326–330.

Al Holo, S., 2005. Etude numérique de la localisation à l'aide de modèles de second gradient: Perte d'unicité et évolution de la taille de la zone localisée. Ph.D. Thesis, Université Joseph Fourier, France.

Bésuelle, P., Chambon, R., Collin, F., 2006. Switching deformation modes in post-localization solutions with a quasibrittle material. Journal of Mechanics of Materials and Structures 1, 1115–1134.

Chambon, R., Caillerie, D., El Hassan, N., 1996. Etude de la localisation unidiemnsionelle à l'aide d'un modèle de second gradient. CRAS Paris 323, 231–238.

Chambon, R., Caillerie, D., El Hassan, N., 1998. One-dimensional localisation studied with a second grade model. Eur. J. Mech. A/Solids 17, 637–656.

Chambon, R., Caillerie, D., Matsushima, T., 2001a. Plastic continuum with microstructure, local second gradient theories for geomaterials: localization studies. International Journal of Solids and Structures 38, 8503–8527.

Chambon, R., Caillerie, D., Tamagnini, C., 2004. A strain space gradient plasticity theory for finite strain. Computer Methods in Applied Mechanics and Engineering 193, 2797–2826.

Chambon, R., Crochepeyre, S., Charlier, R., 2001b. An algorithm and a method to search bifurcation point in non linear problems. Int. J. Numer. Methods Engng. 51, 315–332.

Chambon, R., Moullet, J., 2004. Uniqueness studies in boundary value problem involving some second gradient models. Computer Methods Appl. Mech. Eng. 193, 2771–2796.

Charlier, R., 1987. Approche unifiée de quelques problèmes non linéaires de mécanique des milieux continus par la méthode des éléments finis. Ph.D. Thesis, University of Liège, Belgium.

Crook, T., Willson, S., Guo Yu, J., Owen, R., 2003. Computational modelling of the localized deformation associated with borehole breakout in quasi-brittle materials. Journal of Petroleum Science and Engineering 38, 177–186.

Desrues, J., Chambon, R., Mokni, M., Frédéric, M., 1996. Void ratio evolution inside shear bands in triaxial sand specimens studied by computed tomography. Géotechnique 46, 529–546.

Germain, P., 1973a. La méthode des puissances virtuelle en mécanique des milieux continus: Première partie: théorie du second gradient. Journal de Mécanique 12, 235–274.

Germain, P., 1973b. The method of virtual power in continuum mechanics. Part 2: microstructure. SIAM J. Appl. Math. 25, 556–575.

Lenoir, N., Bornert, M., Desrues, J., Bésuelle, P., Viggiani, G., 2007. Volumetric digital image correlation applied to X-ray micro tomography images from triaxial compression tests on argillaceous rocks. Strain, International Journal for Experimental Mechanics 43, 193–205.

Matsushima, T., Chambon, R., Caillerie, D., 2002. Large strain finite element analysis of a local second gradient model: application to localization. Int. J. Numer. Methods Eng. 54, 499–521.

Mindlin, R., 1964. Micro-structure in linear elasticity. Arch. Ration. Mech. An. 16, 51–78.

Mindlin, R., 1965. Second gradient of strain and surface-tension in linear elasticity. Int. J. Solids Structures 1, 18–35.

Papanastasiou, P., Vardoulakis, I., 1992. Numerical analysis of progressive localization with application to borehole stability. International Journal for Numerical and Analytical Methods in Geomechanics 13, 183–198.

Pijaudier-Cabot, G., Bažant, Z., 1987. Nonlocal damage theory. Journal of Engineering Mechanics, ASCE 113, 1512–1533.

Truesdell, C., Noll, W., 1943. The non linear field theories of mechanics in Encyclopaedia of Physics. Springer Verlag.

Vardoulakis, I., Sulem, J., 1995. Bifurcation Analysis in Geomechanics. Blackie academic and professional.